$CMRO_2$の絶対値定量化に関する病態論的な意義は必ずしも明らかではない．脳虚血の指標としてのCBFやOEFの絶対値に意義を見出すのであれば，検査環境を限りなく統一化し，同一の生理環境を担保する必要がある．多くの臨床的局面においては，定量数値に意味を見出すのではなく，あくまで局所変化を補足する情報として理解することもひとつの考え方である．真に有用な臨床指標と，それを提示する臨床検査プロトコルについて更なる検討が必要と考えられる．

文献

1) Leenders KL, Perani D, Lammertsma AA, et al : Cerebral blood flow, blood volume and oxygen utilization. Normal values and effect of age. Brain **113** (Pt 1) : 27-47, 1990

2) Mintun MA, Raichle ME, Martin WR, et al : Brain oxygen utilization measured with O-15 radiotracers and positron emission tomography. J Nucl Med **25** : 177-187, 1984

3) Iida H, Kanno I, Inugami A, et al : [Continuous-monitoring detector-system of arterial H2(15)O concentration for positron-emission tomography : construction of the system and correction for the dispersion and time-shift]. Kaku igaku The Japanese journal of nuclear medicine **24** : 1587-1594, 1987

4) Kudomi N, Choi E, Yamamoto S, et al : Development of a GSO detector assembly for a continuous blood sampling system. IEEE Trans Nucl Sci **50** : 70-73, 2003

5) Iida H, Higano S, Tomura N, et al : Evaluation of regional differences of tracer appearance time in cerebral tissues using [^{15}O] water and dynamic positron emission tomography. J Cereb Blood Flow Metab **8** : 285-288, 1988

6) Iida H, Kanno I, Miura S, et al : Error analysis of a quantitative cerebral blood flow measurement using $H_2{}^{15}O$ autoradiography and positron emission tomography with respect to the dispersion of the input function. J Cereb Blood Flow Metab **6** : 536-545, 1986

7) Iida H, Jones T, Miura S : Modeling approach to eliminate the need to separate arterial plasma in oxygen-15 inhalation positron emission tomography. J Nucl Med **34** : 1333-1340, 1993

8) Kudomi N, Hayashi T, Watabe H, et al : A physiologic model for recirculation water correction in $CMRO_2$ assessment with $^{15}O_2$ inhalation PET. J Cereb Blood Flow Metab **29** : 355-364, 2009

9) Sasakawa Y, Kudomi N, Yamamoto Y, et al : Omission of [(15)O] CO scan for PET CMRO(2) examination using (15)O-labelled compounds. Ann Nucl Med **25** : 189-196, 2011

10) Ito H, Kanno I, Kato C, et al : Database of normal human cerebral blood flow, cerebral blood volume, cerebral oxygen extraction fraction and cerebral metabolic rate of oxygen measured by positron emission tomography with 15O-labelled carbon dioxide or water, carbon monoxide and oxygen : a multicentre study in Japan. Eur J Nucl Med Mol Imaging **31** : 635-643, 2004

11) Kudomi N, Hayashi T, Teramoto N, et al : Rapid quantitative measurement of $CMRO_2$ and CBF by dual administration of ^{15}O-labeled oxygen and water during a single PET scan-a validation study and error analysis in anesthetized monkeys. J Cereb Blood Flow Metab **25** : 1209-1224, 2005

12) Hattori N, Bergsneider M, Wu HM, et al : Accuracy of a method using short inhalation of (15)O-O(2) for measuring cerebral oxygen extraction fraction with PET in healthy humans. J Nucl Med **45** : 765-770, 2004

13) Yamamoto Y, de Silva R, Rhodes CG, et al : Noninvasive quantification of regional myocardial metabolic rate of oxygen by $^{15}O_2$ inhalation and positron emission tomography. Experimental validation. Circulation **94** : 808-816, 1996

14) Hatazawa J, Fujita H, Kanno I, et al : Regional cerebral blood flow, blood volume, oxygen extraction fraction, and oxygen utilization rate in normal volunteers measured by the autoradiographic technique and the single breath inhalation method. Ann Nucl Med **9** : 15-21, 1995

15) Iida H, Law I, Pakkenberg B, et al : Quantitation of regional cerebral blood flow corrected for partial volume effect using O-15 water and PET : I. Theory, error analysis, and stereologic comparison. J Cereb Blood Flow Metab **20** : 1237-1251, 2000

16) Law I, Iida H, Holm S, et al : Quantitation of regional cerebral blood flow corrected for partial volume effect using O-15 water and PET : II. Normal values and gray matter blood flow response to visual activation. J Cereb Blood Flow Metab **20** : 1252-1263, 2000

17) Mintun MA, Lundstrom BN, Snyder AZ, et al : Blood flow and oxygen delivery to human brain during functional activity : theoretical modeling and experimental data. Proc Natl Acad Sci USA **98** : 6859-6864, 2001

18) Takahashi K : [Regional cerebral blood flow and oxygen consumption during normal human sleep]. No to shinkei = Brain and nerve **41** : 919-925, 1989

Cytotherapy, 2012; 14: 441–450

informa
healthcare

Human umbilical cord provides a significant source of unexpanded mesenchymal stromal cells

AKIE KIKUCHI-TAURA[1,2], AKIHIKO TAGUCHI[1], TAKAYOSHI KANDA[3], TAKAYUKI INOUE[2], YUKIKO KASAHARA[1], HARUKA HIROSE[1], IORI SATO[2], TOMOHIRO MATSUYAMA[4], TAKAYUKI NAKAGOMI[4], KENICHI YAMAHARA[1], DAVID STERN[5], HIROYASU OGAWA[2] & TOSHIHIRO SOMA[2]

[1]*Department of Regenerative Medicine, National Cerebral and Cardiovascular Center, Osaka, Japan,* [2]*Division of Hematology, Department of Internal Medicine, Hyogo College of Medicine, Hyogo, Japan,* [3]*Department of Perinatal Medicine, Osaka Minami Medical Center, Osaka, Japan,* [4]*Institute for Advanced Medical Sciences, Hyogo College of Medicine, Hyogo, Japan, and* [5]*Executive Dean's Office, University of Tennessee, Tennessee, USA*

Abstract

Background aims. Human mesenchymal stromal cells (MSC) have considerable potential for cell-based therapies, including applications for regenerative medicine and immune suppression in graft-versus-host disease (GvHD). However, harvesting cells from the human body can cause iatrogenic disorders and *in vitro* expansion of MSC carries a risk of tumorigenesis and/or expansion of unexpected cell populations. *Methods.* Given these problems, we have focused on umbilical cord, a tissue obtained with few ethical problems that contains significant numbers of MSC. We have developed a modified method to isolate MSC from umbilical cord, and investigated their properties using flow cytometry, mRNA analysis and an *in vivo* GvHD model. *Results.* Our study demonstrates that, using umbilical cord, large numbers of MSC can be safely obtained using a simple procedure without *in vitro* expansion, and these non-expanded MSC have the potential to suppress GvHD. *Conclusions.* Our results suggest that the combined banking of umbilical cord-derived MSC and identical cord blood-derived hematopoietic stem cell banking, where strict inspection of the infectious disease status of donors is performed, as well as further benefits of HLA-matched mesenchymal cells, could become one of the main sources of cells for cell-based therapy against various disorders.

Key Words: *cell banking, graft-versus-host disease, mesenchymal stromal cells, umbilical cord*

Introduction

Mesenchymal stromal cells (MSC) can be obtained from various tissues, including bone marrow (1), adipose tissue (2), trabecular bone (3), synovium (4), pancreas (5), lung, liver, spleen (6), peripheral blood (7), cord blood (8), amniotic fluid and umbilical cord (9–11). MSC include multiple cell types that have the capacity to differentiate into neurons, adipocytes, cartilage, skeletal muscle, hepatocytes and cardiomyocytes, under appropriate conditions across embryonic germ layers (2,12). Cell-based therapies using MSC have been initiated in patients with arthrosis (13), corneal disorders (14), stroke (15) and chronic heart failure (16). MSC are also used to suppress graft-versus-host disease (GvHD) in patients after allogeneic hematopoietic stem cell transplantation, and co-transplantation of hematopoietic cells and MSC to enhance engraftment has provided promising results (17). To broaden the indications for use of MSC against multiple disorders, cell banking with HLA-typing would be desirable.

Although MSC can be obtained from a range of organs, the iatrogenic risks associated with harvesting cells from the human body cannot be denied, particularly with harvesting from the large number of individuals required to establish a cell bank. In contrast, harvesting of cells from umbilical cord carries little risk to the donor, and MSC have been identified in placenta (18), amniotic fluid (19), umbilical cord blood (20) and the umbilical cord itself (21). Furthermore, the omission of *in vitro* expansion offers significant benefits for cell banks with large numbers of samples. The present study focused on the umbilical cord, because of the relative ease of cleaning the tissue before harvest and subsequent isolation of the cells. The umbilical cord is covered by

Correspondence: **Akihiko Taguchi**, Department of Regenerative Medicine, National Cerebral and Cardiovascular Center, 5-7-1 Fujishiro-dai, Suita, Osaka, Japan 565–8565. E-mail: taguchi@ri.ncvc.go.jp

(Received 2 June 2011; accepted 13 January 2012)

ISSN 1465-3249 print/ISSN 1477-2566 online
DOI: 10.3109/14653249.2012.658911

an epithelium derived from the enveloping amnion and contains two arteries and one vein, all of which are surrounded by the mucoid connective tissue of Wharton's jelly. The main role of this jelly-like material is to prevent compression, torsion and bending of the enclosed vessels, which provide bidirectional blood flow between the fetal and maternal circulations. The network of glycoprotein microfibrils and collagen fibrils in Wharton's jelly has already been elucidated (22). The phenotypic stromal cells in Wharton's jelly are fibroblast-like cells (23), morphologically and immunophenotypically similar to MSC isolated from bone marrow (9,24,25). MSC from the umbilical cord have been shown to differentiate into adipocytes, osteocytes, neurons and insulin-producing cells (9,24–30). Carlin *et al.* (31) recently demonstrated embryonic transcription factors, such as octamer-binding transcription factor (Oct)-4, sex determining region Y-box (Sox)-2 and Nanog, in porcine umbilical cord matrix cells. These results indicate that umbilical cord-derived mesenchymal stem (UCMS) cells may represent a major source of cells for cell-based therapy. The present study demonstrates that large numbers of MSC can be obtained from umbilical cord using a simple procedure without *in vitro* expansion. Furthermore, UCMS isolated using this procedure are shown to suppress severe GvHD in a murine model.

Methods

All procedures for the isolation and differentiation of human UCMS cells were approved by the Osaka Minami Medical Center (Osaka, Japan). institutional review board and all volunteer donating mothers provided written informed consent. Animal experiments were carried out in accordance with the guidelines of the Animal Care Committee of Hyogo College of Medicine (Hyogo, Japan). Quantitative analyzes were conducted by an investigator who had been blinded to the experimental protocol, identities of animals and experimental conditions pertaining to the animals under study.

Isolation of UCMS cells

Human umbilical cords were obtained from patients delivered at full-term by Cesarean section ($n = 30$). After collection of cord blood as described previously (32), placenta and umbilical cord were placed into a sterilized bag and the following procedures were performed in a safety cabinet. In this study, we used only umbilical cord tissue for further experiments. Both ends of the umbilical cord (approximately 1 cm from each end) were cut and discarded with the placenta. The remaining umbilical cord was immersed and washed in 80% ethanol for 1 min, rinsed with sterile saline twice and cut into approximately 10-cm lengths. Cord blood and blood clots in the umbilical cord artery were removed by flushing twice, using a 20-G tip cut needle, sterile saline and 20-mL syringe. Then the umbilical cord segments were immersed and washed with 80% ethanol for 1 min, followed by two rinses with sterile saline. Next, the umbilical cord was cut into 2–4-cm lengths and the epithelial tissue was removed using sterilized scissors. The remaining tissue was incubated in an enzyme cocktail solution, containing 1 mg/mL hyaluronidase (Sigma-Aldrich, St Louis, MO, USA), 300 U/mL collagenase (Sigma-Aldrich) and 3 mM $CaCl_2$ (Wako Pure Chemical Industries, Osaka, Japan) in Dulbecco's modified Eagle's medium (DMEM) (Invitrogen, Carlsbad, CA, USA) for 2 h at 37°C with shaking (50 shakes/min; BR-21UM; Taitec, Saitama, Japan). After incubation, undigested vascular components were removed and the tissue solution was crushed with forceps and passed through 180- and 125-μm diameter stainless steel mesh (Tokyo Screen, Tokyo, Japan), followed by 70-μm diameter mesh (Becton Dickinson, Franklin Lakes, NJ, USA), to remove large pieces of unlysed tissue. The tissue solution was then collected by centrifugation (200 ***g*** for 5 min) and resuspended in phosphate-buffered saline (PBS). The latter washing procedure was performed twice. Next, the tissue solution was incubated with 0.5% trypsin–ethylenediamine tetraacetic acid. (EDTA) (Invitrogen) in PBS for 1 h at 37°C. After trypsinization, the tissue solution was neutralized with 2% fetal bovine serum (FBS) in DMEM and this washing procedure was performed twice. As a control, the conventional method of tissue preparation reported by Weiss *et al.* (29) was used to isolate UCMS cells. That procedure is similar to our own, the major difference being that we did not remove the umbilical artery from the umbilical cord before digestion with hyaluronidase and collagenase.

Flow cytometric analysis of UCMS cells

Antigens expressed by freshly isolated and *in vitro*-expanded and -differentiated umbilical cord-derived cells were investigated by multicolor flow cytometry. The expression of surface markers in 1×10^5 cells was analyzed. The characteristics of each antibody are listed in Table I. As a control, a non-immune isotype control (Beckman Coulter Orange County, CA, USA) was employed.

Expansion and in vitro *differentiation of UCMS cells*

To investigate the properties of isolated UCMS cells as MSC, cells were expanded *in vitro* as described previously (29). Briefly, 1×10^4 cells/cm^2 were plated in a low-serum media, containing 56% low-glucose DMEM (Invitrogen), 37% MCDB201

Table I. Antibodies for flow cytometry.

Antigen	Label	Manufacturer	Catalog number
CD11b	FITC	Beckman Coulter	IM1284
CD14	FITC	Beckman Coulter	IM0645
CD19	FITC	Beckman Coulter	IM1284
CD29	FITC	Beckman Coulter	6604105
CD31	FITC	BD	555445
CD34	PC7	Beckman Coulter	A21691
CD34	PC5	Beckman Coulter	A07777
CD38	FITC	Beckman Coulter	IM0775
CD44	PE[a]	Beckman Coulter	IM0845
CD45	FITC	Beckman Coulter	A07782
CD45	ECD	Beckman Coulter	A07784
CD73	Biotin[b]	BD	550256
CD90	PE	Beckman Coulter	IM1840
CD105	PE	Beckman Coulter	A07414
CD117	PE	Beckman Coulter	IM2732
CD133	PE	Miltenyi Biotec	130-080-901
GlycophorinA	PE	Beckman Coulter	IM2211
HLA-DR	FITC	BD	555560
vWF	FITC*	Beckman Coulter	IM0150

[a]Antibody was labeled with a Zenon Mouse IgG1 labeling kit (Invitrogen).
[b]Biotin-labeled antibody was detected by strept avidin–PC5.
FITC, fluorescein isothiocyanate; PE, phycoerythrin; PC, phycoerythrin-cyanin; ECD, phycoerythrin-TexasRED. BD, Becton Dickinson, Franklin Lakes, NJ, USA, Mitenyi Biotec; Bergisch Gladbach, Nordrhein-Westfalen, Germany

(Sigma-Aldrich), 2% FBS (StemCell Technologies, Vancouver, Canada), 1 × insulin-transferrin-selenium-X (ITS-X; Invitrogen), 1 × ALBU-Max I (Invitrogen), 1 × antibiotics-antimycotics (Invitrogen), 10 nM dexamethasone (Sigma-Aldrich), 50 μM ascorbic acid 2-phosphate (Sigma-Aldrich), 1 ng/mL epidermal growth factor (EGF; Peprotech, Rocky Hill, NJ, USA) and 10 ng/mL platelet-derived growth factor-BB (PDGF-BB; (R&D Systems, Minneapolis, MN, USA). After reaching 70–80% confluence, cells were replated at 20% confluence.

After cell expansion (passage 2), 70% confluent UCMS cells were differentiated into neuronal cells, adipocytes, osteocytes, chondrocytes, myoblasts, and pancreatic cells, as described previously (33–36). Briefly, prior to neuronal induction, UCMS cells were grown overnight in DMEM with 20% FBS (Invitrogen) and 10 ng/mL basic fibroblast growth factor (Peprotech). Cells were rinsed twice with PBS and incubated in DMEM with 100 μM butylated hydroxyanisole (BHA; Sigma-Aldrich), 10 μM forskolin (Sigma-Aldrich), 2% dimethyl sulfoxide (DMSO; Sigma-Aldrich), 5 U/mL heparin (Fuso Pharmaceutical Industries, Osaka, Japan), 5 nM K252a (Sigma-Aldrich), 25 mM KCl (Wako Pure Chemical Industries), 2 mM valproic acid (Sigma-Aldrich) and 1 × N2 supplement (Invitrogen). For differentiation into adipocytes, UCMS cells were incubated in DMEM with 1 μM dexamethasone, 0.5 mM 3-isobutyl-1-methlxanthine (Sigma-Aldrich), 1 μg/mL insulin (Sigma-Aldrich) and 100 μM indomethacin (Sigma-Aldrich). Differentiated cells were stained with Oil Red O (Sigma-Aldrich). For differentiation into osteocytes, UCMS cells were incubated in osteogenic differentiation medium in accordance with the manufacturer's protocol for 31 days (Invitrogen). Differentiated cells were stained with Alizarin Red S (Sigma-Aldrich). To investigate the potential formation of a chondrogenic pellet, UCMS cells were incubated in chondrogenic differentiation medium according to the manufacturer's protocol for 21 days (Invitrogen). Differentiated cell pellets were stained with Alcian Blue (Sigma-Aldrich) and cross-sections were studied. For differentiation into myoblasts, UCMS cells were initially incubated in DMEM with 2% FBS, 10 ng/mL EGF, 10 ng/mL PDGF-BB and 3 μM 5-azacytidine (Sigma-Aldrich) for 24 h. The medium was then changed to DMEM with 2% FBS, 10 ng/mL EGF and 10 ng/mL PDGF-BB. For differentiation into pancreatic cells, UCMS cells were cultured for 7 days in RPMI-1640 medium (Sigma-Aldrich) with 5% FBS and 10 mmol/L nicotinamide (Sigma-Aldrich). Cells were then cultured for an additional 5 days in the presence of 10 nM exendin 4 (Sigma-Aldrich).

Total RNA extraction and reverse transcriptase–polymerase chain reaction analysis

Total RNA was extracted from freshly isolated and *in vitro*-differentiated UCMS cells using RNeasy purification reagent (Qiagen, Hilden, Germany). Reverse transcriptase–polymerase chain reaction (RT-PCR) analysis was performed using a SuperScript One-Step RT-PCR System (Invitrogen) with 100 ng of tRNA. Sequences and annealing temperatures for each primer are described in Table II. The amplified cDNA was separated by electrophoresis through a 2% agarose gel, stained with ethidium bromide, and photographed under ultraviolet light.

GvHD model

Female B6C3F1 (recipient; C57BL/6 × C3H/He; H-$2^{b/k}$) and BDF1 (donor; C57BL/6 × DBA/2; H-$2^{b/d}$) mice between 8 and 12 weeks old were purchased from Japan SLC (Shizuoka, Japan). Mice were housed in sterile micro-isolator cages in a pathogen-free facility with *ad libitum* access to autoclaved food and hyperchlorinated drinking water. Donor bone marrow cells were harvested from tibiae and femurs by flushing with RPMI-1640 medium (Sigma-Aldrich). Recipient mice were lethally irradiated with 13 Gy total body irradiation (TBI; X-ray) split into two doses separated by 3 h. This amount of radiation and dose of infused donor cells has been shown to

Table II. Sequence of RT-PCR primers.

Gene	5′-primer	3′-primer	Temp. (°C)
Osteopontin	CTAGGCATCACCTGTGCCATACC	CAGTGACCAGTTCATCAGATTCATC	60
ALP	TCAGAAGCTCAACACCAACG	GTCAGGGACCTGGGCATT	51
Sox-9	ACATCTCCCCCAACGCCATC	TCGCTTCAGGTCAGCCTTGC	51
Aggrecan	TGCGGGTCAACAGTGCCTATC	CACGATGCCTTTCACCACGAC	51
PPARγ2	GCATTATGAGACATCCCCACTGC	CCTATTGACCCAGAAAGCGATTC	59
GFAP	CTGGGCTCAAGCAGTCTACC	AATTGCCTCCTCCTCCATCT	58
MAP-2	CTGCTTTACAGGGTAGCACAA	TTGAGTATGGCAAACGGTCTG	58
MyoD	GCTAGGTTCACGTTTCTCGC	GCGCCTTTATTTTGATCACC	58
Glucagon	GAGGGCTTGCTCTCTCTTCA	GTGAATGTGCCCTGTGAATG	57

ALP, alkaline phosphatase; GFAP, glial fibrillary acidic protein; MAP, microtubule-associated protein PPAR, peroxisome proliferator-activated receptor..

induce GvHD after hematopoietic stem cell transplantation (37). On the following day, donor-derived cells (1×10^7 bone marrow cells and 2×10^7 spleen cells) were suspended in 0.2 mL RPMI-1640 medium and transplanted via the tail vein into post-irradiation recipient mice. Soon after hematopoietic stem cell transplantation, 1×10^6 non-expanded and non-selected UCMS cells in 0.2 mL RPMI medium were transplanted via the tail vein. In the control group, the same amount of RPMI was infused via the tail vein. On day 7 after transplantation, the same number of non-expanded UCMS cells or RPMI medium alone was injected via the tail vein into treated mice or control mice, respectively. The severity of GvHD was evaluated using a scoring system incorporating five clinical parameters, as described previously (38): body weight; posture (hunching); mobility; fur texture; and skin integrity. Mice were evaluated and graded from 0 to 2 for each criterion. A clinical index was subsequently generated by summation of the five criteria scores (38). A score of 0–5 was defined as mild GvHD and a score of 6–10 or dead was defined as severe GvHD.

Statistical analysis

Statistical comparisons were performed using a Student's *t*-test or χ^2 test. For all experiments,

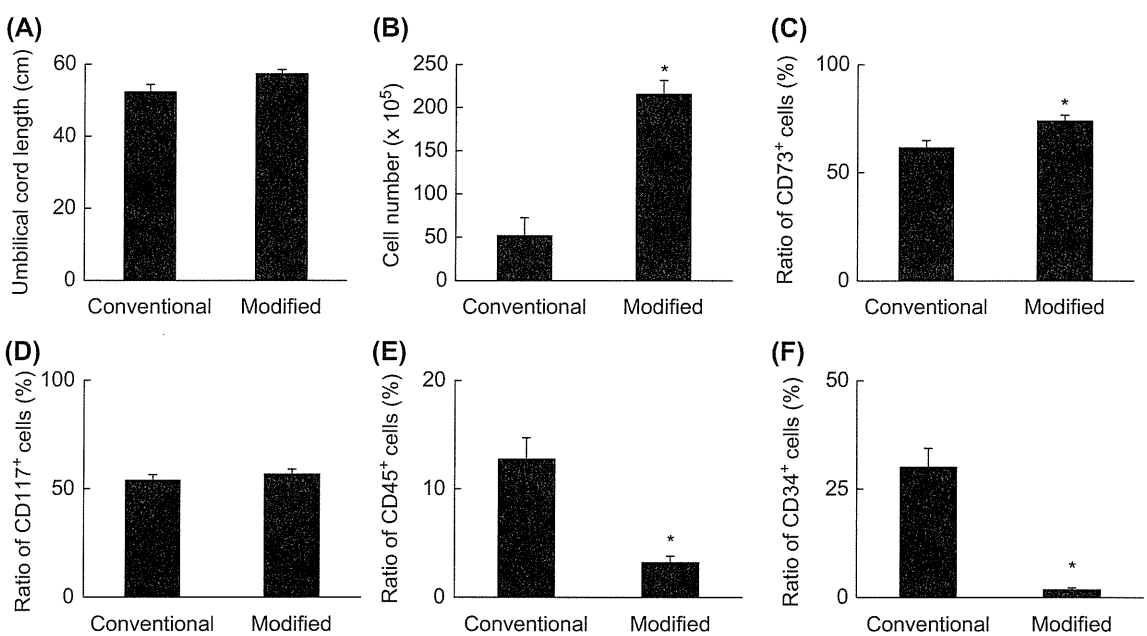

Figure 1. Cell numbers and characteristics of isolated MSC. No significant difference in the length of the umbilical cord was seen between groups (A). The total number of cells obtained with our modified method (216×10^5 cells) was more than 4-fold greater, compared with the conventional method (52×10^5 cells) (B). A significant increase in the ratio of cells expressing an MSC marker (CD73) was observed with the modified method (74.1%), compared with the conventional method (61.8%) (C). In contrast, no significant difference was observed in CD117-positive cells between modified (56.9%) and conventional methods (54.1%) (D). Contamination by cells from the hematopoietic lineage, expressing CD45 (E) and CD34 (F), was significantly decreased with the modified method (3.2% and 1.9%, respectively), compared with the conventional method (12.8% and 30.1%, respectively). *$P < 0.05$ versus conventional method.

values are reported as mean ± standard error of the mean. Values of $P < 0.05$ were considered statistically significant.

Results

Characterization of isolated UCMS cells

MSC were isolated from umbilical cord using either conventional methods (29) ($n = 12$) or our modified methodology ($n = 18$). Although no significant differences in the length of umbilical cords were observed (Figure 1A), more than four times as many cells were obtained using our method (Figure 1B). To investigate the characteristics of these cells, surface cell markers were analyzed by flow cytometry for CD73, as an MSC marker (Figure 1C); a significant increase in the ratio of CD73-positive MSC was observed using our method, compared with the conventional technique. In contrast, no significant difference in the ratio of cells positive for the stem cell marker CD117 was identified between groups (Figure 1D). Umbilical cord contains a range of cell types, including hemocytes and endothelial cells. To investigate the level of these cells in our final cell population, numbers of CD45- and CD34-positive cells were investigated by flow cytometry (CD45, Figure 1E; CD34, Figure 1F). We observed a significant reduction in contamination by endothelial cells using our modified methodology compared with the conventional technique.

To evaluate properties of freshly isolated umbilical cord-derived cells, cell surface markers were analyzed by multiple staining for cell-surface markers. As shown in Figure 2, only a small fraction of CD73-positive cells displayed hemocyte/hematopoietic cell markers, including anti-CD11b, CD14, CD19, CD34, CD38, CD45, CD133, GlycophorinA and HLA-DR. These results indicated that the CD73-positive cell fraction contained a low level of hemocyte or hematopoietic cells. To evaluate the presence of endothelial cells in the CD73-positive cell fraction, the expression of various endothelial cell markers, including CD31, CD34 and von Willebrand Factor (vWF), was investigated; the majority of CD73-positive cells were negative for these endothelial cell markers. To confirm our results, expression of CD90, a marker not present on endothelial cells (39), was evaluated; more than 95% of CD73-positive cells expressed CD90. These findings indicated little contamination by endothelial cells using our modified methodology and were consistent with the visual impression that most vascular components remained undigested after incubation with hyaluronidase and collagenase for 2 h.

Changes in cell-surface markers of isolated umbilical cord-derived cells after in vitro expansion

To evaluate further the character of the isolated cell population, freshly prepared umbilical cord-derived cells using our modified methodology were cultured up to passage 4. Expanded cells showed a spindle-shaped morphology (Figure 3A) that associated with common MSC. Analysis of cell-surface markers revealed that expression of CD44 (Figure 3B; a cell-surface glycoprotein involved in cell–cell interactions expressed by mesenchymal cells), CD105 (Figure 3C; a membrane glycoprotein expressed

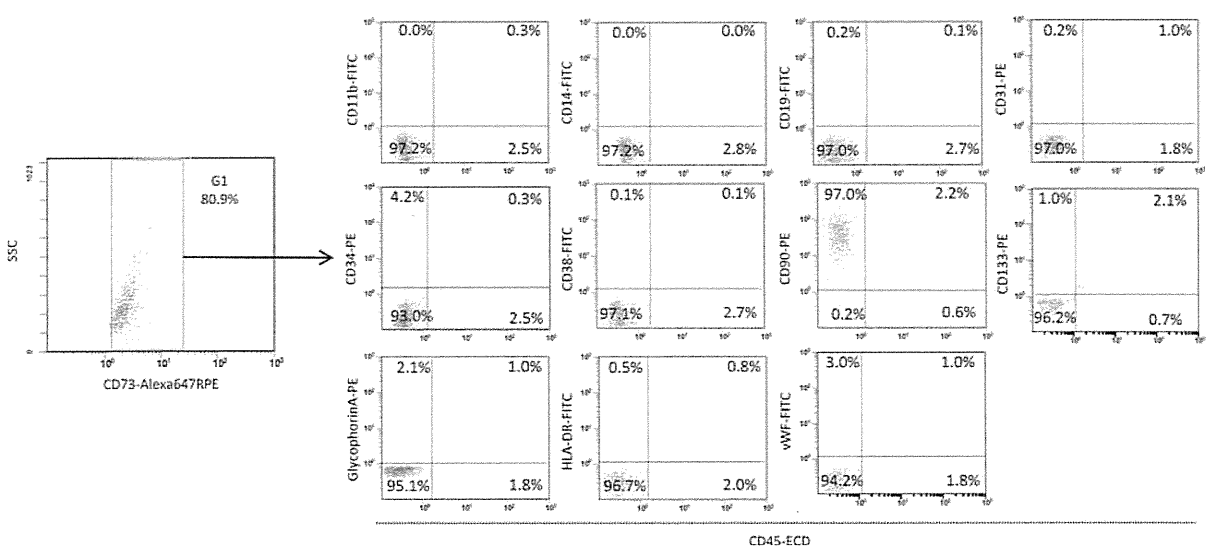

Figure 2. Multicolor analysis of freshly isolated MSC obtained by the modified protocol. To evaluate the presence of non-MSC, surface markers of freshly isolated cells were investigated. The majority of CD73-positive cells were negative for markers of hemocyte (CD11b, CD14, CD19, CD34, CD38, CD133, GlycophorinA, HLA-DR) and endothelial cell (CD31, vWF) lineages. It is notable that most of the CD73-positive cells expressed CD90, the latter not expressed on endothelial cells.

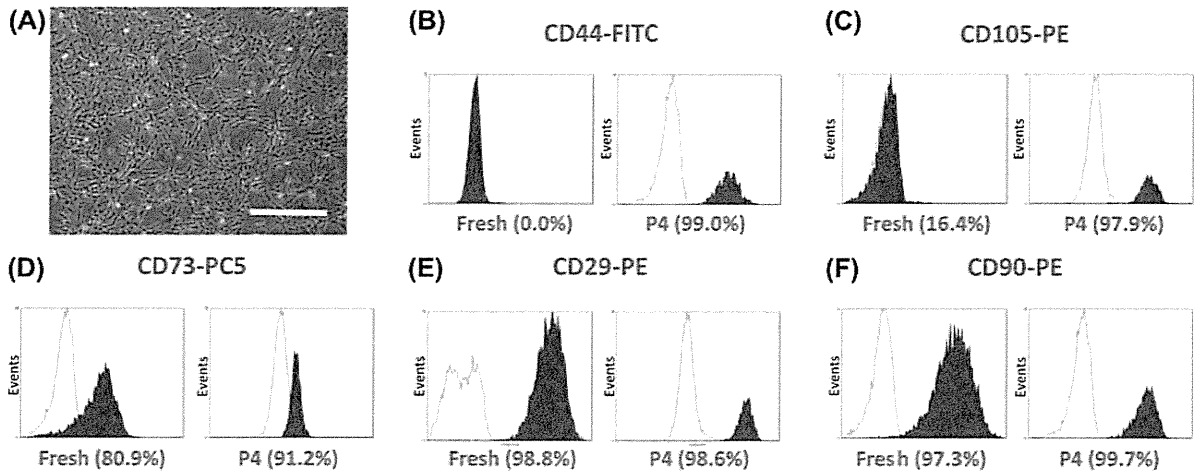

Figure 3. Changes in cell-surface markers associated with *in vitro* expansion. (A) Phase-contrast image of expanded UCMS cells. After *in vitro* expansion, analysis of MSC markers revealed an increased expression of CD44 (B), CD105 (C) and CD73 (D). In contrast, no change was observed in the expression of CD29 (E) and CD90 (F) because of *in vitro* expansion. Scale bar, 100 μm (A).

in multiple cell types including mesenchymal cells) and CD73 (Figure 3D; a nucleotidase expressed by multiple cells including mesenchymal cells) was increased in cells at passage 4. In contrast, expression of CD29 (Figure 3E; an integrin expressed in MSC) and CD90 (Figure 3F; a glycophosphatidylinositol-anchored cell-surface protein expressed by multiple cells including MSC) was similar to that observed prior to *ex vivo* expansion. These profiles were similar to amniotic-derived MSC as reported by De Coppi *et al.* (40).

Potential of UCMS cells

To investigate the potential of isolated UCMS cells to form differentiated cell types, the cell population was expanded under conditions conducive for osteocyte, chondrocyte or adipogenic differentiation. Under conditions conducive to the formation of osteocytes, on day 31 in cell culture Alizarin Red S-positive mineralized matrix-like nodules were observed (Figure 4A) and analysis of RNA confirmed the expression of osteocyte markers, osteopontin and alkaline phosphatase (ALP) (Figure 4B). Similarly, under conditions conducive to formation of a chondrogenic pellet, on day 21 in cell culture, Alcian Blue-positive chondrogenic-like pellets were observed (Figure 4C) and analysis of RNA confirmed the expression of chondrocyte markers, Sox-9 and aggrecan (Figure 4D). Under conditions leading to the formation of adipocytes, on day 20 of cell culture, Oil Red O-positive cells with lipid droplets were observed (Figure 4E, F) and analysis of RNA confirmed the expression of adipocyte marker peroxisome proliferator-activated receptor PPARγ2 (Figure 4G). Similarly, isolated cells incubated under conditions leading to neuronal differentiation showed subsequent expression of microtubule-associated protein 2 (MAP-2) and glial fibrillary acidic protein (GFAP) (Figure 4H). Furthermore, differentiated UCMS cells showed the myocyte marker MyoD (Figure 4I) and glucagon as a pancreatic cell marker (Figure 4J) when incubated under conditions leading to the formation of myocytes and pancreatic cells, respectively.

Suppression of GvHD by UCMS cells transplantation

In vitro-expanded MSC have been shown to suppress GvHD in patients after hematopoietic stem cell transplantation (41). To evaluate the potential for non-expanded UCMS cells to suppress GvHD, mice underwent allogeneic hematopoietic stem cell transplantation and were treated with non-expanded UCMS cells in RPMI. As a control, mice underwent allogeneic hematopoietic stem cell transplantation and were treated with RPMI alone. Mice were treated with non-expanded UCMS on days 0 and 6 after allogeneic stem cell transplantation, and the survival rate and severity of GvHD were investigated by 25 weeks after Bone Marrow Transplantation. (BMT). The frequency of severe GvHD at 6 weeks after allogeneic stem cell transplantation was significantly reduced with concomitant transplantation of non-expanded UCMS cells (Figure 4A). Although all mice in the control group showed severe GvHD or were already dead at 6 weeks, none of those treated with non-expanded UCMS cells (after the second treatment) were dead or showed severe GvHD. Representative pictures at 6 weeks in control and UCMS groups are shown in Figure 4B, C, respectively. Figure 4D shows the survival curve after allogeneic hematopoietic stem cell transplantation. Although no

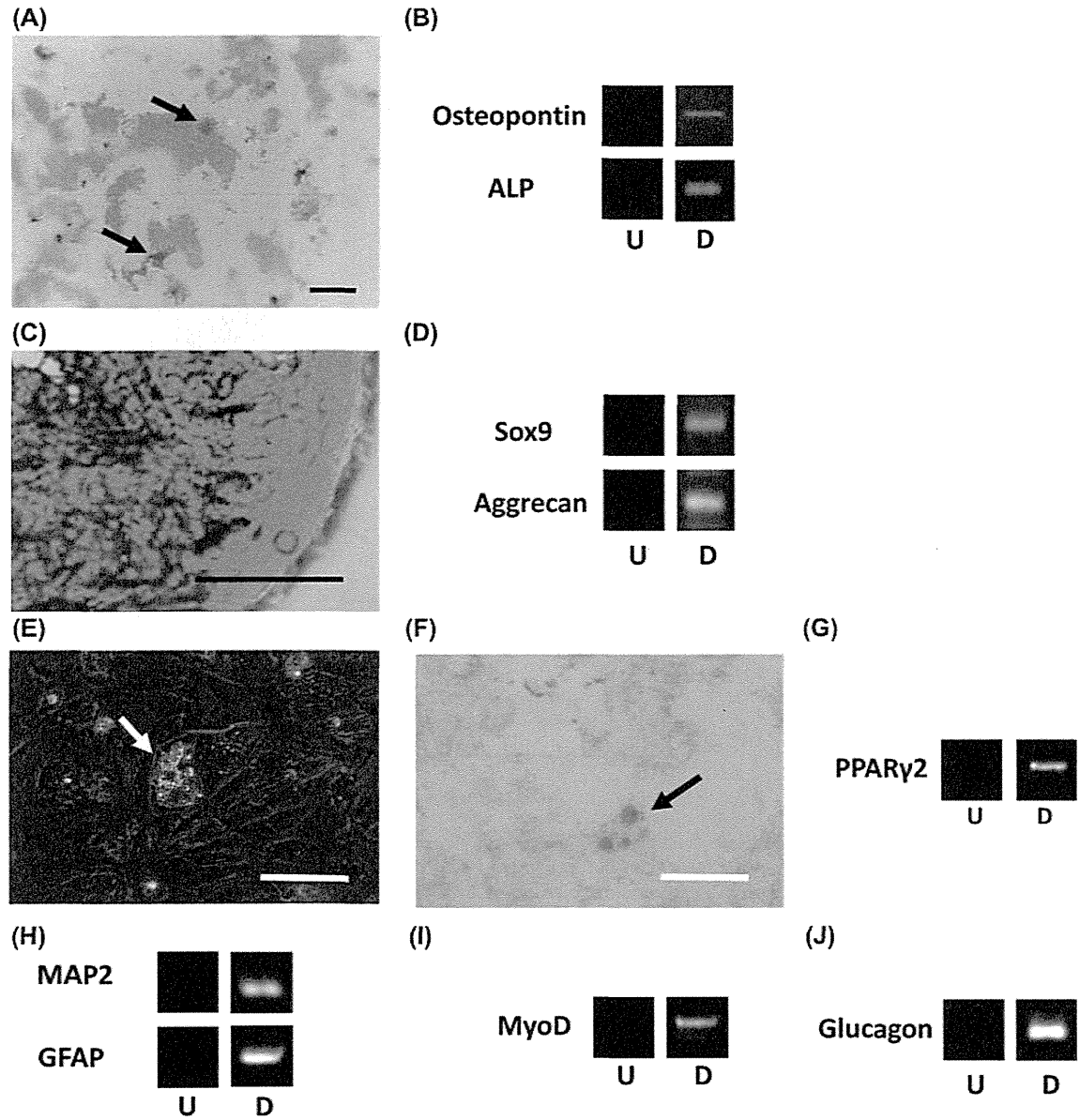

Figure 4. *In vitro* differentiation of freshly isolated UCMS cells. After expansion under conditions conducive to osteocyte or chondrocyte differentiation, Alizarin Red S-positive mineralized matrix-like nodules (A) or Alcian Blue-positive chondrogenic-like pellets (the latter displayed formation of layered structure at the surface) (C), respectively, were observed. UCMS cells cultured under conditions conductive to differentiation of osteocyte (B) and chondrocyte (D) cells expressed specific markers for each lineage. After expansion under conditions conducive to adipocyte differentiation, Oil Red O-positive adipocytes (E, phase-contrast image; F, Oil Red O staining) were observed and expression of PPARγ2 was observed (G). UCMS cells cultured under conditions conductive to differentiation of neuronal (H), myocyte (I) and pancreas (J) cells expressed specific markers for each lineage. Each experiment was repeated five times using different umbilical cord-derived cells. Scale bar, 40 μm (A), 100 μm (C, E, F). The arrow indicates Alizarin Red S-positive mineralized matrix-like nodules (A), lipid droplet (E) and Oil Red O-positive cells (F). U, undifferentiated; D, differentiated (B, D, G–J).

significant difference was apparent between groups at the 4-week assessment point, all of the mice in the control group were dead in 25 weeks, whereas no death was observed in mice with UCMS treatment group after the second treatment (Figure 5D).

Discussion

This study demonstrates that more than 2×10^7 MSC can be obtained safely from human umbilical cord without *in vitro* expansion and that these non-expanded MSC have the potential to suppress GvHD.

As a source of MSC, the umbilical cord has major advantages, including little contamination by cells of maternal origin, easy sterilization and few ethical problems. Compared with the method described by Weiss *et al.* (29), our modified method omits removal of blood vessels from the umbilical cord before treatment with collagenase and hyaluronidase.

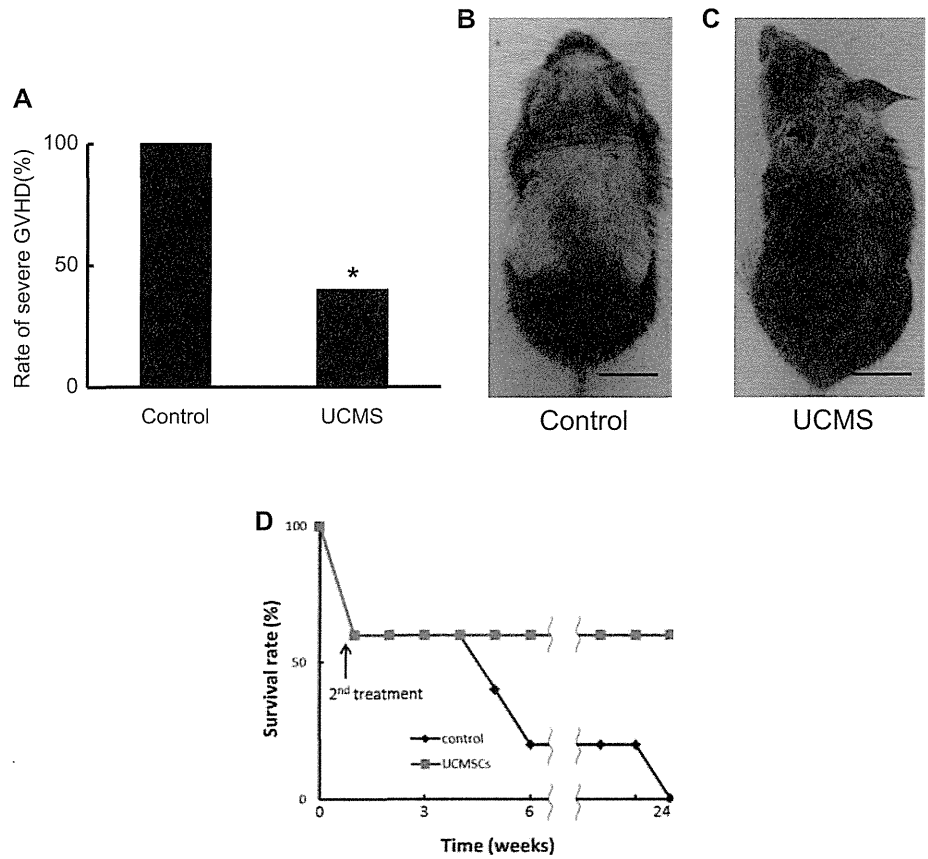

Figure 5. Suppression of GvHD by UCMS cells transplantation. Although all mice in the control group died or showed severe GvHD at 6 weeks (score 6; 1 mouse, dead; 4 mice), treatment with non-expanded UCMS cells significantly reduced the severity of GvHD (score 3; 1 mouse, score 4; 2 mice, dead; 2 mice) (A). Representative pictures of animals from the control group (B) and non-expanded UCMS cell-treated group (C) are shown. (D) Survival curve after radiation and allogeneic hematopoietic stem cell transplantation ($n = 5$, in each group). All of the mice in the control group were dead by 25 weeks after allogeneic hematopoietic stem cell transplantation. In contrast, no mice in the UCMS group were dead after the second infusion of non-expanded UCMS cells. $^*P < 0.05$ versus control. Scale bar, 1 cm (B, C).

Removal of the umbilical artery results in the loss of Wharton's jelly, which contains significant numbers of MSC. Preservation of the blood vessels before digestion with collagenase and hyaluronidase also significantly reduced contamination by endothelial cells. This finding may be attributed to removal of intact vascular structures from the cell suspension before digestion with trypsin, as vasculature was not considerably degraded in the presence of collagenase and hyaluronidase according to our protocol. Furthermore, our method has a significant advantage in that no *in vitro* cell culture is required for isolation of MSC from umbilical cord. In contrast, recently published methods described by Capelli *et al.* (11) and Lu *et al.* (10) involve cell culture over several days for isolation of MSC. The advantage of protocols using *in vitro* expansion is that non-adhesive cells can be removed, resulting in an enriched adhesive cell population. However, our results indicate that freshly isolated and non-selected umbilical cord-derived cells obtained by our method suppressed GvHD in an animal model. *In vitro* expansion of MSC carries a risk of tumorigenesis (42) and clinical use of the expanded cells requires strict monitoring to ensure safety. Our modified method has significant advantages in the reduced time required for the isolation procedure and its safety, both of which are important for cell banking. For the studies reported here, we used only the umbilical cords obtained at full-term Cesarean sections. It is likely that the properties and number of MSC in umbilical cord are similar comparing Cesarean section and vaginal delivery. Although caution should be taken regarding cleanliness/sterility after vaginal delivery, we expect that the same procedure can be used for umbilical cords obtained at full-term vaginal delivery.

In addition to offering a cell source for regenerative medicine, MSC have the potential to suppress GvHD after hematopoietic stem cell transplantation. Although the mechanisms and actual cell fraction underlying suppression of GvHD by MSC transplantation remains contentious (43), our results indicate

that human umbilical cord-derived non-expanded MSC suppressed GvHD in a murine model. The optimal type of MSC for suppression of GvHD, in terms of source, level of maturity and HLA-matching to the donor, is unclear. However, our results indicate that non-expanded UCMS cells represent a potential candidate cell source, particularly when co-banked with cord blood-derived hematopoietic cells (provided there is also strict control for contamination with infectious agents with HLA-typing). Furthermore, co-transplantation of HLA-matched hematopoietic stem cells and MSC may be advantageous to reduce clearance of transplanted MSC via immunologic recognition of HLA-matched hematopoietic cells.

In conclusion, our results indicate that umbilical cord-derived non-expanded MSC represent a potential cell source for cell banking and subsequent therapeutic use. Our results indicate that the combination of banking UCMS cells with identical cord blood-derived hematopoietic stem cells could be an important source for cell-based therapies in a range of settings.

Acknowledgments

This work was supported by a Grant-in-Aid for Scientific Research from the Ministry of Health, Labour and Welfare.

Declaration of interest: The authors declare no conflict of interest.

References

1. Liechty KW, MacKenzie TC, Shaaban AF, Radu A, Moseley AM, Deans R, et al. Human mesenchymal stem cells engraft and demonstrate site-specific differentiation after in utero transplantation in sheep. Nat Med. 2000;6:1282–6.
2. Schaffler A, Buchler C. Concise review. Adipose tissue-derived stromal cells: basic and clinical implications for novel cell-based therapies. Stem Cells. 2007;25:818–27.
3. Noth U, Osyczka AM, Tuli R, Hickok NJ, Danielson KG, Tuan RS. Multilineage mesenchymal differentiation potential of human trabecular bone-derived cells. J Orthop Res. 2002;20:1060–9.
4. De Bari C, Dell'Accio F, Luyten FP. Human periosteum-derived cells maintain phenotypic stability and chondrogenic potential throughout expansion regardless of donor age. Arthritis Rheum. 2001;44:85–95.
5. Hu Y, Liao L, Wang Q, Ma L, Ma G, Jiang X, et al. Isolation and identification of mesenchymal stem cells from human fetal pancreas. J Lab Clin Med. 2003;141:342–9.
6. in't Anker PS, Noort WA, Scherjon SA, Kleijburg-van der Keur C, Kruisselbrink AB, van Bezooijen RL, et al. Mesenchymal stem cells in human second-trimester bone marrow, liver, lung, and spleen exhibit a similar immunophenotype but a heterogeneous multilineage differentiation potential. Haematologica. 2003;88:845–52.
7. Huss R, Lange C, Weissinger EM, Kolb HJ, Thalmeier K. Evidence of peripheral blood-derived, plastic-adherent CD34(–/low) hematopoietic stem cell clones with mesenchymal stem cell characteristics. Stem Cells. 2000;18:252–60.
8. Rogers I, Casper RF. Umbilical cord blood stem cells. Best Pract Res Clin Obstet Gynaecol. 2004;18:893–908.
9. Romanov YA, Svintsitskaya VA, Smirnov VN. Searching for alternative sources of postnatal human mesenchymal stem cells: candidate MSC-like cells from umbilical cord. Stem Cells. 2003;21:105–10.
10. Lu LL, Liu YJ, Yang SG, Zhao QJ, Wang X, Gong W, et al. Isolation and characterization of human umbilical cord mesenchymal stem cells with hematopoiesis-supportive function and other potentials. Haematologica. 2006;91:1017–26.
11. Capelli C, Gotti E, Morigi M, Rota C, Weng L, Dazzi F, et al. Minimally manipulated whole human umbilical cord is a rich source of clinical-grade human mesenchymal stromal cells expanded in human platelet lysate. Cytotherapy. 2011;13:786–801.
12. Bjorklund A, Lindvall O. Cell replacement therapies for central nervous system disorders. Nat Neurosci. 2000;3:537–44.
13. Galle J, Bader A, Hepp P, Grill W, Fuchs B, Kas JA, et al. Mesenchymal stem cells in cartilage repair: state of the art and methods to monitor cell growth, differentiation and cartilage regeneration. Curr Med Chem. 2010;17:2274–91.
14. Liu H, Zhang J, Liu CY, Wang IJ, Sieber M, Chang J, et al. Cell therapy of congenital corneal diseases with umbilical mesenchymal stem cells: lumican null mice. PLoS One. 2010;5:1–4.
15. Lee JS, Hong JM, Moon GJ, Lee PH, Ahn YH, Bang OY. A long-term follow-up study of intravenous autologous mesenchymal stem cell transplantation in patients with ischemic stroke. Stem Cells. 2010;28:1099–106.
16. Schuleri KH, Feigenbaum GS, Centola M, Weiss ES, Zimmet JM, Turney J, et al. Autologous mesenchymal stem cells produce reverse remodelling in chronic ischaemic cardiomyopathy. Eur Heart J. 2009;30:2722–32.
17. Lim JH, Lee MH, Yi HG, Kim CS, Kim JH, Song SU. Mesenchymal stromal cells for steroid-refractory acute graft-versus-host disease: a report of two cases. Int J Hematol. 2010;92:204–7.
18. Portmann-Lanz CB, Schoeberlein A, Huber A, Sager R, Malek A, Holzgreve W, et al. Placental mesenchymal stem cells as potential autologous graft for pre- and perinatal neuroregeneration. Am J Obstet Gynecol. 2006;194:664–73.
19. in't Anker PS, Scherjon SA, Kleijburg-van der Keur C, Noort WA, Claas FH, Willemze R, et al. Amniotic fluid as a novel source of mesenchymal stem cells for therapeutic transplantation. Blood. 2003;102:1548–9.
20. Erices A, Conget P, Minguell JJ. Mesenchymal progenitor cells in human umbilical cord blood. Br J Haematol. 2000;109:235–42.
21. Wang HS, Hung SC, Peng ST, Huang CC, Wei HM, Guo YJ, et al. Mesenchymal stem cells in the Wharton's jelly of the human umbilical cord. Stem Cells. 2004;22:1330–7.
22. Meyer FA, Laver-Rudich Z, Tanenbaum R. Evidence for a mechanical coupling of glycoprotein microfibrils with collagen fibrils in Wharton's jelly. Biochim Biophys Acta. 1983;755:376–87.
23. McElreavey KD, Irvine AI, Ennis KT, McLean WH. Isolation, culture and characterisation of fibroblast-like cells derived from the Wharton's jelly portion of human umbilical cord. Biochem Soc Trans. 1991;19:29S.
24. Covas DT, Siufi JL, Silva AR, Orellana MD. Isolation and culture of umbilical vein mesenchymal stem cells. Braz J Med Biol Res. 2003;36:1179–83.

25. Sarugaser R, Lickorish D, Baksh D, Hosseini MM, Davies JE. Human umbilical cord perivascular (HUCPV) cells: a source of mesenchymal progenitors. Stem Cells. 2005;23:220–9.
26. Fu YS, Shih YT, Cheng YC, Min MY. Transformation of human umbilical mesenchymal cells into neurons in vitro. J Biomed Sci. 2004;11:652–60.
27. Fu YS, Cheng YC, Lin MY, Cheng H, Chu PM, Chou SC, et al. Conversion of human umbilical cord mesenchymal stem cells in Wharton's jelly to dopaminergic neurons in vitro: potential therapeutic application for Parkinsonism. Stem Cells. 2006;24:115–24.
28. Kadivar M, Khatami S, Mortazavi Y, Shokrgozar MA, Taghikhani M, Soleimani M. In vitro cardiomyogenic potential of human umbilical vein-derived mesenchymal stem cells. Biochem Biophys Res Commun. 2006;340:639–47.
29. Weiss ML, Medicetty S, Bledsoe AR, Rachakatla RS, Choi M, Merchav S, et al. Human umbilical cord matrix stem cells: preliminary characterization and effect of transplantation in a rodent model of Parkinson's disease. Stem Cells. 2006;24: 781–92.
30. Chao KC, Chao KF, Fu YS, Liu SH. Islet-like clusters derived from mesenchymal stem cells in Wharton's jelly of the human umbilical cord for transplantation to control type 1 diabetes. PLoS One. 2008;3:1–9.
31. Carlin R, Davis D, Weiss M, Schultz B, Troyer D. Expression of early transcription factors Oct-4, Sox-2 and Nanog by porcine umbilical cord (PUC) matrix cells. Reprod Biol Endocrinol. 2006;4:1–13.
32. Rubinstein P, Dobrila L, Rosenfield RE, Adamson JW, Migliaccio G, Migliaccio AR, et al. Processing and cryopreservation of placental/umbilical cord blood for unrelated bone marrow reconstitution. Proc Natl Acad Sci USA. 1995;92:10119–22.
33. Woodbury D, Reynolds K, Black IB. Adult bone marrow stromal stem cells express germline, ectodermal, endodermal, and mesodermal genes prior to neurogenesis. J Neurosci Res. 2002;69:908–17.
34. Dennis JE, Merriam A, Awadallah A, Yoo JU, Johnstone B, Caplan AI. A quadripotential mesenchymal progenitor cell isolated from the marrow of an adult mouse. J Bone Miner Res. 1999;14:700–9.
35. Reyes M, Lund T, Lenvik T, Aguiar D, Koodie L, Verfaillie CM. Purification and ex vivo expansion of postnatal human marrow mesodermal progenitor cells. Blood. 2001;98:2615–25.
36. Tang DQ, Cao LZ, Burkhardt BR, Xia CQ, Litherland SA, Atkinson MA, et al. In vivo and in vitro characterization of insulin-producing cells obtained from murine bone marrow. Diabetes. 2004;53:1721–32.
37. Taniguchi Y, Yoshihara S, Hoshida Y, Inoue T, Fujioka T, Ikegame K, et al. Recovery from established graft-vs-host disease achieved by bone marrow transplantation from a third-party allogeneic donor. Exp Hematol. 2008;36:1216–25.
38. Cooke KR, Kobzik L, Martin TR, Brewer J, Delmonte J Jr, Crawford JM, et al. An experimental model of idiopathic pneumonia syndrome after bone marrow transplantation. I. The roles of minor H antigens and endotoxin. Blood. 1996;88:3230–9.
39. Mutin M, Dignat-George F, Sampol J. Immunologic phenotype of cultured endothelial cells: quantitative analysis of cell surface molecules. Tissue Antigens. 1997;50:449–58
40. De Coppi P, Bartsch G Jr, Siddiqui MM, Xu T, Santos CC, Perin L, et al. Isolation of amniotic stem cell lines with potential for therapy. Nat Biotechnol. 2007;25:100–6.
41. Le Blanc K, Frassoni F, Ball L, Locatelli F, Roelofs H, Lewis I, et al. Mesenchymal stem cells for treatment of steroid-resistant, severe, acute graft-versus-host disease: a phase II study. Lancet. 2008;371:1579–86.
42. Spaeth EL, Dembinski JL, Sasser AK, Watson K, Klopp A, Hall B, et al. Mesenchymal stem cell transition to tumor-associated fibroblasts contributes to fibrovascular network expansion and tumor progression. PLoS One. 2009; 4:1–11.
43. Sato K, Ozaki K, Mori M, Muroi K, Ozawa K. Mesenchymal stromal cells for graft-versus-host disease : basic aspects and clinical outcomes. J Clin Exp Hematop. 2010;50:79–89.

In Vitro Cell.Dev.Biol.—Animal (2012) 48:143–148
DOI 10.1007/s11626-012-9486-z

REPORT

Mouse ES cells maintained in different pluripotency-promoting conditions differ in their neural differentiation propensity

Haruka Hirose · Hidemasa Kato · Akie Kikuchi-Taura · Toshihiro Soma · Akihiko Taguchi

Received: 23 November 2011 / Accepted: 8 January 2012 / Published online: 27 January 2012 / Editor: T. Okamoto

Abstract Prior to differentiation, embryonic stem (ES) cells in culture are maintained in a so-called "undifferentiated" state, allowing derivation of multiple downstream cell lineages when induced in a directed manner, which in turn grants these cells their "pluripotent" state. The current work is based on a simple observation that the initial culture condition for maintaining mouse ES cells in an "undifferentiated" state does impact on the differentiation propensity of these cells, in this case to a neuronal fate. We point out the importance in judging the "pluripotency" of a given stem cell culture, as this clearly demonstrated that the "undifferentiated" state of these cells is not necessarily a "pluripotent" state, even for a widely used mouse ES cell line. We partly attribute this difference in the initial value of ES cells to the naïve-to-primed status of pluripotency, which in turn may affect early events of the differentiation in vitro.

Keywords Embryonic stem cell · Culture media · Naïve · Primed · *Fgf5*

H. Hirose · A. Kikuchi-Taura · A. Taguchi
Department of Regenerative Medicine,
National Cerebral and Cardiovascular Center,
5-7-1 Fujishiro-dai,
Suita, Osaka, Japan 565-8565

H. Kato (✉)
Division of Developmental Biology, Research Center for Genomic Medicine, Saitama Medical University,
1397-1 Yamane,
Hidaka, Saitama, Japan 350-1241
e-mail: hidekato@saitama-med.ac.jp

T. Soma
Division of Hematology, Department of Internal Medicine,
Hyogo College of Medicine,
1-1 Mukogawachou,
Nishinomiya, Hyogo, Japan 663-850

A. Taguchi
Department of Regenerative Medicine Research,
Institute of Biomedical Research and Innovation,
2-2 Minatojima Minamimachi Chuo-ku,
Kobe, Hyogo, Japan 650-0047

Introduction

The use of embryonic stem (ES) cells has spread from a classical tool for gene targeting toward models whereby we can test their in vitro developmental properties (in a hope to be reproduced in human systems) for potential therapeutic uses. Previously, the ultimate task for mouse ES cells was to commit into the germ cell lineage when implanted into blastocysts in order to produce transgenic animals. However, the current favorable destinations have been widened up to cells of various organs including brain, heart, pancreas, liver, and many more because of the anticipation toward regenerative medicine. As a consequence, the fashion and requirements to maintain "pluripotent" ES cells are to be modified. Also, if these cells are considered to be directly transplanted into human host organs, concerns naturally rise to avoid animal-derived components (such as mouse feeder cells or bovine serum). To this purpose, a number of serum-free/chemically defined media has been developed from various groups (Furue et al. 2005; Tsuji et al. 2008; Chen et al. 2011).

ES cells are artificial cell entities trapped in a "quasi-eternal" moratorium state for development. In the case of mouse ES cells, this characteristic is mainly endowed by leukemia inhibitory factor (LIF) through its STAT3-activating property (Matsuda et al. 1999). Also, LIF is acting to inhibit MAP kinase activation, which is known to be necessary for the successive development to occur (Hirai et al. 2011). This cell state in which ES cells are

stabilized for self-renewal is now understood as the "ground state" (Ying et al. 2008). The cells in this ground state are considered to be "naïve" (Nichols and Smith 2009) as they are refractory to spontaneous differentiation and self-renew (Ying et al. 2008) without any requirement of mitogen. In contrast, upon LIF removal, ES cells are expected to be swiftly primed for differentiation, a condition also coined "primed" by Smith and colleagues (Nichols and Smith 2009). A suitable condition for ES cell culture is therefore to stably maintain the naïve state during cell expansion but be able to swiftly switch to a primed condition when needed. To date, however, a prospective evaluation of this "switch ability" has not been reported.

Recently, it has been shown that this ground state varies among different mouse strains. It is now considered that the often-used 129 mouse background to derive ES cells has an exceptional property to create a stable ground state (Suzuki et al. 1999). In other strains of mice, this ground state is inherently less stable and hence is now called metastable (Hanna et al. 2009), which explains the difference in the efficiency in deriving ES cell lines from various mouse genetic backgrounds (Suzuki et al. 1999).

We have previously reported a highly reproducible neural induction protocol for mouse ES cells (Bouhon et al. 2005, 2006), which fits well the proposed developmental model of "default neurogenesis" (Hemmati-Brivanlou and Melton 1997; Chang and Hemmati-Brivanlou 1998) originally described for amphibians.

Our study provides evidence that quality control of ES cells for their pluripotency can be only achieved through the incorporation of developmental stage evaluation, especially vis-à-vis the ground state, and also that it may vary according to the aimed cell lineage.

Materials and methods

ES cell culture. Throughout this study, we have used a mouse ES cell line CMTI-1, derived from 129svev mouse background, known to be relatively less dependent to mouse embryonic fibroblast (MEF) feeder cells. However, for the routine maintenance of these cells, the cultures were performed on MEF feeder layer to ensure their pluripotency. ES cells were cultured in Dulbecco's modified eagle medium containing 15% fetal bovine serum (FBS), 1,000 U/ml leukemia inhibitory factor (LIF; Millipore, Billerica, MA), 100 μM 2-mercaptoethanol, 0.03% L-glutamine, 1 mM sodium pyruvate, 100 μM non-essential amino acid, 50 U/ml penicillin, and 50 μg/ml streptomycin (ES cell medium). We routinely split ES cells every other day and replate them at 2.4×10^6 cells/100-mm gelatinized-culture dish. ES cells were gently dispersed using 0.01% trypsin/0.1 mM EDTA in PBS at room temperature by triturating using pipettes. After neutralizing trypsin activity, the cells were collected by centrifugation and resuspended in a fresh medium before plating. To convert from serum-supplemented (SS) to serum-free (SF) media, we adopted the method of "sequential adaptation" suggested by the manufacturer of a widely used compound which substitutes serum in the culture of ES cells, Knockout Serum Replacement (KSR; Invitrogen, Carlsbad, CA) which is also used in the current study or ESFC (Cell Science and Technology Institute, Inc., Tokyo, Japan; Furue et al. 2005). These media were also supplemented with 1,000 U/ml LIF.

Our serum-free adaptation culture steps comprise of starting from a completely serum-supplemented medium, culture media were diluted out using each non-serum media by ratios as follows; Serum media : non-serum media=1:0 (zeroth passage), 3:1 (first passage), 1:1 (second passage), 1:3 (third passage), 1:9 (fourth passage), and ultimately to completely non-serum media (fifth passage onward).

RT-PCR. Total RNA was purified from cells harvested at indicated time points by using RNeasy Micro Kit (QIAGEN, the Netherlands). One microgram of total RNA was used for reverse transcription reaction with Omniscript Reverse Transcriptase (QIAGEN) and Oligo-dT Primer (Invitrogen).

PCR was carried out with TaKaRa Ex Taq Hot Start Version (TaKaRa, Shiga, Japan) and primers listed in Table 1. Each reaction was performed according to manufacturer's protocol. PCR products were electrophoresed in agarose gel and visualized by ethidium bromide.

Induction of neural progenitors from ES cells. SF/feeder-free-adapted ES cells were trypsinized and then neural induction was performed in non-adherent dishes in Chemically Defined Medium (CDM) as described previously (Bouhon et al. 2005, 2006). CDM is a non-instructive developmentally neutral medium consisting of Iscove's Modified Dulbecco's Medium, Ham's F-12 containing polyvinyl alcohol (final concentration 0.1%), holo-transferrin, 1-thioglycerol, insulin, GlutaMAX and a mixture of chemically defined lipids. Suspended cells formed aggregates and were collected and analyzed at day 8 of differentiation when the aggregates contain neural progenitors and some neurite-extending mature neurons. A minor modification to our reported paper is the inclusion of a cell dissociation step at day 4 using Accumax to reduce cell heterogeneity.

Results

Serum-free, feeder-free adaptation culture of ES cells. Commercially available 129svev-derived mouse ES cells (CMTI-1), which can be stably maintained in a serum-containing medium under a non-feeder condition, were used

Table 1. RT-PCR primers used in this study

Gene	Forward primer	Reverse primer
Oct3/4	GGCTTCAGACTTCGCCTCC	AACCTGAGGTCCACAGTATGC
Nanog	TCTTCCTGGTCCCCACAGTTT	GCAAGAATAGTTCTCGGGATGAA
Zfp42/Rex 1	CCCTCGACAGACTGACCCTAA	TCGGGGCTAATCTCACTTTCAT
Fgf5	TGTGTCTCAGGGGATTGTAGG	AGC TGTTTTCTTGGAATCTCTC C
Nestin	CCCTGAAGTCGAGGAGCTG	CTGCTGCACCTCTAAGCGA
Musa.shi	CCTCTCACGGCTTATGGGC	CTGTGGCAATCAAGGGACC
Neurogenin2	AAC TCCACGTCC CCATACAG	GAGGCG CATAACGATGCTTCT
Gata6	ACCTTATGGC GTAGAAAT GC TGAGGGTG	C TGAAJAC TTGAGGTCACTGTTCTCGGG
Kff4	CC GGC GGGAAGGGAGAAGACAC TGCGT	GTGGGTTAGCGAGTTGGAAAGGATAAA
NeuroD 1	CGCCTACAGCGCAGCTCTGG	CGTCGCTGCAGGGTAGTGCA
Ascli	GCTGCAAACGCCGGCTCAAC	GCGGATGTACTCGACCGCCG
Dkk 1	GTCCAAGATCTGTAAACC	GAGTCAAGACAATCAACC
Actb	GGCTGTATTCCCCTCCATCG	CCAGTTGGTAACAATGCCATGT
Gapdh	AGGTC GGTGTGAACGGATTTG	TGTAGAC CATGTAGTTGAGGTCA

throughout the study. To enable direct comparison of the neural differentiation propensities of the same ES cells maintained in different pluripotency-promoting conditions, mouse ES cells cultured under serum-containing medium condition (which represents a routine lab culture condition) were parallely adapted toward two non-serum culture conditions (C-KSR and C-ESFC) as depicted in Fig. 1*a*. From a single ES cell-confluent mouse embryonic fibroblasts (MEF)-fed culture dish in serum-containing media, the two conditions were processed in parallel for ES cell propagation. In Fig 1*a*, C-KSR and C-ESFC depict the sequential adaptation conditions to the KSR-supplemented and ESFC

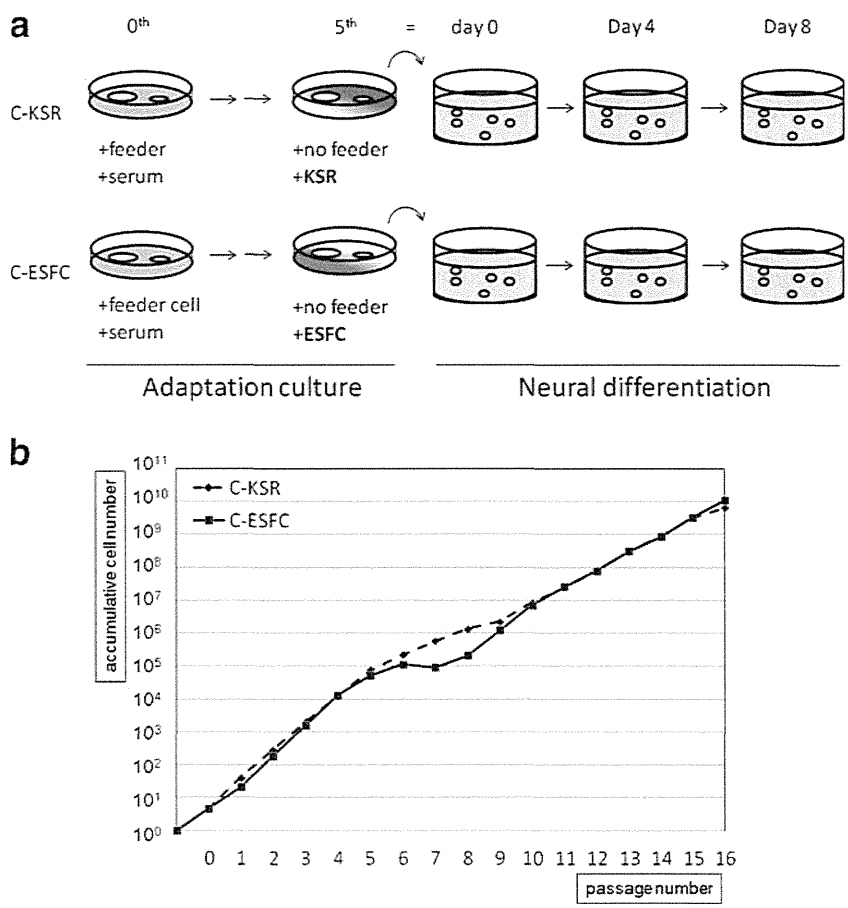

Figure 1. (*a*) Schematic drawing of our experiment depicting the parallel adaptation procedure followed by neural differentiation. Starting from a single MEF feeder ES cell dish (zeroth), cultures were serially adapted in parallel to non-serum medium with KSR (C-KSR) or ESFC (C-ESFC). At the fifth passage, cultures are completely serum-free and were subjected to differentiation into neural progenitor cells. (*b*) A representative cell growth profile during prolonged cell cultures in either KSR or ESFC. Cell proliferation rate as well as cell morphology (data not shown) did not change significantly between condition C-KSR and C-ESFC indicating that both media sustain ES cell self-renewal for a long culture period.

SF media, respectively. As hinted by its manufacturer and observed elsewhere, we found difficulties in efficiently propagating ES cells when the culture was directly transferred into the KSR medium without the adaptation steps probably due to "culture shock" (data not shown). After five passages, both groups were considered to be "adapted" as the culture media are then completely converted to serum-free conditions and virtually no residual MEFs have been observed (see "Materials and methods" for details). All conditions were with leukemia inhibitory factor (LIF; ESGRO; Millipore) at 1,000 unit/mL.

Figure 1*b* shows representative growth profiles of the ES cells under the two culture conditions. Both culture media maintained ES cell proliferation for at least 16 passages (Fig. 1*b*) without any sign of overt differentiation judged by microscopic observation. Both groups showed comparative growth rates throughout the adaptation culture procedure. Interestingly, a combined effect of the serum-containing and SF medium on cell proliferation has been observed (approximately in the fifth passage). This is in good accordance with the idea that the factors supplemented in each SF medium, provides independent mechanisms for ES cell growth (which cannot be substituted at least with factors present in the serum used in this study). Although cell and colony morphology was largely similar between C-KSR- and C-ESFC-cultured cells (Fig. 1*b*), we found a tendency for C-ESFC-cells to form "domed" colonies.

We therefore concluded at this step that the two culture conditions used in this study are comparable for their cell proliferative capacities.

Comparative analyses of the pluripotency markers in undifferentiated ES cells. To comparatively analyze the pluripotency of the ES cells under the two different conditions, the expression levels of classical pluripotency markers, that are *Pou5f1* (also called *Oct-3/4*), *Nanog*, *Klf4*, *Zfp42* (also called *Rex1*), were evaluated. These transcription factors have been repeatedly shown to be essential for the pluripotency of the ES cells by creating a core transcriptional network (Kim et al. 2008). RT-PCR analyses showed no obvious difference in the expression levels of core pluripotency factors *Pou5f1*, *Sox2*, and *Nanog* before differentiation (KSR D0 and ESFC D0 columns in Fig. 2). However, we found significant differences for the expression of *Zfp42*, and *Klf4* (Fig. 2). As the latter two markers are representative for naïve ES cells (Nichols and Smith 2009), we next turn our attention to a primitive ectoderm marker, *Fgf5*, which can discriminate the two distinct states of ES cells, which are naïve versus primed. By semi-quantitative RT-PCR, we observed that ES cells in the C-ESFC have significantly higher level of *Fgf5* expression before differentiation (Fig. 2). Judging by these results, we

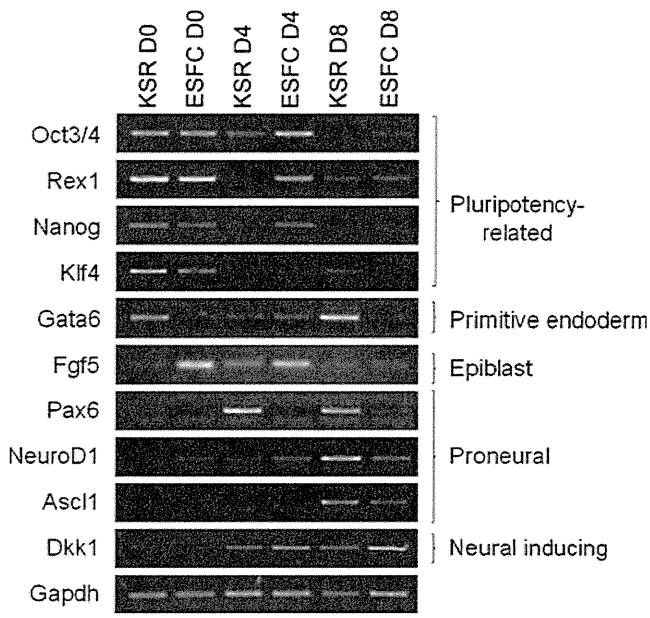

Figure 2. Developmentally regulated gene expression during the parallel differentiation of ES cells maintained either in KSR- or ESFC-media. At the start of differentiation (D0), pluripotency-related markers (*Nanog*, *Rex1*, *Oct3/4*, and *Klf4*) were both positive under condition C-KSR and C-ESFC. Major differences in marker expression at this undifferentiated stage were observed for a primitive endodermal marker *Gata6* and for a primitive ectoderm/epiblast marker *Fgf5*. At D4 of differentiation, pluripotency-related factor's expression (Oct3/4, Rex1, and Nanog) persisted only in ESFC-derived cells which may signify a delayed differentiation or a residual population of undifferentiated cells. Interestingly, an early neuroectodermal marker *Pax6* was only turned on from KSR-cells. Consistently, at D8 of differentiation when the majority of cells within the differentiating spheres are expected to be of neural characters (Bouhon et al. 2005), only KSR-derived cells expressed *Pax6* as well as other proneural markers such as *NeuroD1* and *Ascl1*. The gene expression levels for the neural-inducing agent Dkk1 were even for both groups if not higher for the neural-recalcitrant ESFC-derived cells.

tentatively interpret that culture condition C-KSR tends to maintain ES cells in a naïve state compared to C-ESFC condition, which in turn seems to retain these cells in a more primed state.

Naïve-to-primed balance impacts on the neural induction efficiency of ES cells. A strong motivation which led us to this current study was our empirical observation that neural induction starting from mouse ES cells highly depended on the initial undifferentiated state of the culture. Even mouse ES cells with less dependency on feeder cells, such as 129Ola- or 129svev-derived ES cells, exhibit abnormal morphologies upon prolonged culture. This was observed without necessarily changing their expression profiles for the pluripotency-related markers such as *Oct3/4*, *Sox2* or *Nanog* (data not shown). We knew that this tendency was almost always accompanied with poor differentiation outputs. We

therefore reasoned that ES cell properties apart from the core pluripotency factors' statuses would influence such differentiation propensities. To this end, we in vitro differentiated in parallel, ES cells cultured either in condition C-KSR or C-ESFC (remaining columns in Fig. 2). The differentiation protocol we have independently developed has a characteristic similar to the "default model" of early embryonic cell differentiation (Chang and Hemmati-Brivanlou 1998; see "Discussion"). As shown in Fig. 2, we observed a distinct transcriptional regulation for *Pax6*, which is an early marker for our default neural progenitor cells (Bouhon et al. 2006). In addition, the proneural genes *NeuroD1* and *Ascl1* (also called *Mash1*) showed strongly biased expression in favor of C-KSR-derived cells. In addition, *Musashi1* and *Neurogenin2* also showed similar tendencies (data not shown). When we turn our attention to the pluripotency-related markers, we surprisingly found that C-ESFC condition exhibits a resistance for this differentiation judging by residual expression of *Pou5f1*, *Nanog*, *Rex1*, and *Fgf5* (see for examples, expression levels of *Pou5f1* and *Nanog* in ESFC D4 samples).

It is also noteworthy that the neural-inducing activities of *Dkk1*, an antagonist of Wnt activity expressed from a non-neural cell lineage transiently present in our differentiation culture, seem comparable between the two groups in terms of expression level and/or timing.

Discussion

Hochedlinger and coworkers have pinpointed epigenetic alterations which impair induced pluripotent stem (iPS) cells from their full developmental potentials (Stadtfeld et al. 2010). Surprisingly, they have spotted a gene locus which is governed by genetic imprinting but with no implication to pluripotency. This represents a good example implying that the "superficial" pluripotency, judged by expression of restricted number of markers is not sufficient to predict full developmental potential.

In this work, we have observed that the expressivity of *Fgf5* could serve for such a predictive marker for developmental potential, at least to a neural cell lineage, provided that the core pluripotency markers (*Pou5f1*, *Sox2*, and *Nanog*) are present. *Fgf5* is exclusively expressed in epiblast and in epiblast stem cells which are derived from it (Pelton et al. 2002). However, in a recent work, its expression has also been demonstrated in cells at their "primed" state for differentiation (Nichols and Smith 2009). This indicates that the differentiation efficiency using a specific induction protocol is influenced by not only the superficial pluripotent state but also the different degree of "priming" for differentiation. Our current study is indicative that this variety of differentiation priming is a consequence of the culture environment, in this case, the culture media, as all other conditions have been equalized. In the future, it would therefore be necessary to manipulate the cell culture system of ES cell, prior to its differentiation, according to the aimed cell lineage. To this end, the effort presented in this work should also be extended for other cell lineages than neural.

The reason why a "primed-like" condition (C-ESFC) was more refractory to neural differentiation would warrant further investigation. Our previous observation in which we showed that a transient contribution of primitive endoderm lineage was present during this neural differentiation might explain this puzzling situation. As *Fgf5* expression is suggestive that the cells are more committed toward an epiblast-like stage, high expressors of *Fgf5* may be more recalcitrant to produce primitive endoderm lineage cells, which segregate earlier during development from epiblast primitive ectoderm (Lu et al. 2001). Although *Dkk1* which is mainly expressed from the anterior visceral endoderm, a descendant of the primitive endoderm, is equally expressed in both conditions during differentiation, the possibility that the neural-inducing cell populations differ between the two groups merits further investigation. An important observation of our study is that markers which are indicative of an undifferentiated state of ES cells disappeared more slowly in C-ESFC. Because the primed state in the developmental context signifies its readiness to differentiate, this cannot be easily reconciled with the idea that C-ESFC is more "primed" or more advanced in the developmental schedule (judged by *Fgf5* expression). This implication that the cells in a certain condition do not enter the neural fate within the due duration of the experiment could be because of delayed lineage choice or because the cells have entered a distinct state from which they cannot reach the neural fate. This observation would warrant deeper investigation in the future if one is to prospectively judge the developmental propensities of a given stem cell line or to evaluate and determine the proper initial characteristics of the iPS cells generated.

At the very least, our finding is suggestive that most cell differentiation protocols are highly sensitive to a subtle difference in the developmental stages of ES cells which cannot be easily standardized if the culture conditions of ES cells differ from lab to lab. This may also explain the encountered difficulties in reproducing cell differentiation protocols by different labs.

Acknowledgments H. K. thanks Nick Allen for sharing unpublished data related to the neural differentiation protocol and for the long-term friendship. We all thank Yosuke Moriyama for critically reading the manuscript. This work was supported by Grants-in-Aid for Scientific Research on Innovative Areas (KAKENHI 23111008) awarded to H. K.

References

Bouhon I. A.; Joannides A.; Kato H.; Chandran S.; Allen N. D. Embryonic stem cell-derived neural progenitors display temporal restriction to neural patterning. *Stem Cells* 24: 1908–1913; 2006.

Bouhon I. A.; Kato H.; Chandran S.; Allen N. D. Neural differentiation of mouse embryonic stem cells in chemically defined medium. *Brain Res. Bull.* 68: 62–75; 2005.

Chang C.; Hemmati-Brivanlou A. Cell fate determination in embryonic ectoderm. *J. Neurobiol.* 36: 128–151; 1998.

Chen G.; Gulbranson D. R.; Hou Z.; Bolin J. M.; Ruotti V.; Probasco M. D.; Smuga-Otto K.; Howden S. E.; Diol N. R.; Propson N. E.; Wagner R.; Lee G. O.; Antosiewicz-Bourget J.; Teng J. M.; Thomson J. A. Chemically defined conditions for human iPSC derivation and culture. *Nat. Methods* 8: 424–429; 2011.

Furue M.; Okamoto T.; Hayashi Y.; Okochi H.; Fujimoto M.; Myoishi Y.; Abe T.; Ohnuma K.; Sato G. H.; Asashima M.; Sato J. D. Leukemia inhibitory factor as an anti-apoptotic mitogen for pluripotent mouse embryonic stem cells in a serum-free medium without feeder cells. *In Vitro Cell. Dev. Biol. Anim.* 41: 19–28; 2005.

Hanna J.; Markoulaki S.; Mitalipova M.; Cheng A. W.; Cassady J. P.; Staerk J.; Carey B. W.; Lengner C. J.; Foreman R.; Love J.; Gao Q.; Kim J.; Jaenisch R. Metastable pluripotent states in NOD-mouse-derived ESCs. *Cell Stem Cell* 4: 513–524; 2009.

Hemmati-Brivanlou A.; Melton D. Vertebrate neural induction. *Annu. Rev. Neurosci.* 20: 43–60; 1997.

Hirai H.; Karian P.; Kikyo N. Regulation of embryonic stem cell self-renewal and pluripotency by leukaemia inhibitory factor. *Biochem. J.* 438: 11–23; 2011.

Kim J.; Chu J.; Shen X.; Wang J.; Orkin S. H. An extended transcriptional network for pluripotency of embryonic stem cells. *Cell* 132: 1049–1061; 2008.

Lu C. C.; Brennan J.; Robertson E. J. From fertilization to gastrulation: axis formation in the mouse embryo. *Curr. Opin. Genet. Dev.* 11: 384–392; 2001.

Matsuda T.; Nakamura T.; Nakao K.; Arai T.; Katsuki M.; Heike T.; Yokota T. STAT3 activation is sufficient to maintain an undifferentiated state of mouse embryonic stem cells. *EMBO J.* 18: 4261–4269; 1999.

Nichols J.; Smith A. Naive and primed pluripotent states. *Cell Stem Cell* 4: 487–492; 2009.

Pelton T. A.; Sharma S.; Schulz T. C.; Rathjen J.; Rathjen P. D. Transient pluripotent cell populations during primitive ectoderm formation: correlation of in vivo and in vitro pluripotent cell development. *J. Cell Sci.* 115: 329–339; 2002.

Stadtfeld M.; Apostolou E.; Akutsu H.; Fukuda A.; Follett P.; Natesan S.; Kono T.; Shioda T.; Hochedlinger K. Aberrant silencing of imprinted genes on chromosome 12qF1 in mouse induced pluripotent stem cells. *Nature* 465: 175–181; 2010.

Suzuki O.; Matsuda J.; Takano K.; Yamamoto Y.; Asano T.; Naiki M.; Kusanagi M. Effect of genetic background on establishment of mouse embryonic stem cells. *Exp. Anim.* 48: 213–216; 1999.

Tsuji Y.; Yoshimura N.; Aoki H.; Sharov A. A.; Ko M. S.; Motohashi T.; Kunisada T. Maintenance of undifferentiated mouse embryonic stem cells in suspension by the serum- and feeder-free defined culture condition. *Dev. Dyn.* 237: 2129–2138; 2008.

Ying Q. L.; Wray J.; Nichols J.; Batlle-Morera L.; Doble B.; Woodgett J.; Cohen P.; Smith A. The ground state of embryonic stem cell self-renewal. *Nature* 453: 519–523; 2008.

Neurochemistry International 61 (2012) 240–250

Contents lists available at SciVerse ScienceDirect

Neurochemistry International

journal homepage: www.elsevier.com/locate/nci

Linkage of N-cadherin to multiple cytoskeletal elements revealed by a proteomic approach in hippocampal neurons

Hidekazu Tanaka [a,*], Kazuaki Takafuji [a], Akihiko Taguchi [b], Pattama Wiriyasermkul [a], Ryuichi Ohgaki [a], Shushi Nagamori [a], Pann-Ghill Suh [c], Yoshikatsu Kanai [a]

[a] Department of Pharmacology, Osaka University School of Medicine, Osaka 565-0871, Japan
[b] Institute of Biomedical Research and Innovation, Kobe 650-0047, Japan
[c] Advanced Research Center for Signal Transduction in Cancers, Ulsan National Institute of Science and Technology, Ulsan 689-798, Republic of Korea

ARTICLE INFO

Article history:
Received 5 April 2012
Received in revised form 7 May 2012
Accepted 9 May 2012
Available online 17 May 2012

Keywords:
Synapse
Plasticity
Adhesion
Cadherin
Cytoskeleton
Hippocampus

ABSTRACT

The CNS synapse is an adhesive junction differentiated for chemical neurotransmission and is equipped with presynaptic vesicles and postsynaptic neurotransmitter receptors. Cell adhesion molecule cadherins not only maintain connections between pre- and postsynaptic membranes but also modulate the efficacy of synaptic transmission. Although the components of the cadherin-mediated adhesive apparatus have been studied extensively in various cell systems, the complete picture of these components, particularly at the synaptic junction, remains elusive. Here, we describe the proteomic assortment of the N-cadherin-mediated synaptic adhesion apparatus in cultured hippocampal neurons. N-cadherin immunoprecipitated from Triton X-100-solubilized neuronal extract contained equal amounts of β- and α-catenins, as well as F-actin-related membrane anchor proteins such as integrins bridged with α-actinin-4, and Na^+/K^+-ATPase bridged with spectrins. A close relative of β-catenin, plakoglobin, and its binding partner, desmoplakin, were also found, suggesting that a subset of the N-cadherin-mediated adhesive apparatus also anchors intermediate filaments. Moreover, dynein heavy chain and LEK1/CENPF/mitosin were found. This suggests that internalized pools of N-cadherin in trafficking vesicles are conveyed by dynein motors on microtubules. In addition, ARVCF and NPRAP/neurojungin/δ2-catenin, but not p120ctn/δ1-catenin or plakophilins-1, -2, -3, -4 (p0071), were found, suggesting other possible bridges to microtubules. Finally, synaptic stimulation by membrane depolarization resulted in an increased 93-kDa band, which corresponded to proteolytically truncated β-catenin. The integration of three different classes of cytoskeletal systems found in the synaptic N-cadherin complex may imply a dynamic switching of adhesive scaffolds in response to synaptic activity.

1. Introduction

The CNS synapse is an adhesive junction differentiated for chemical transmission and is equipped with presynaptic vesicles and postsynaptic neurotransmitter receptors. Cell adhesion molecules that link pre- and postsynaptic membranes not only maintain specific synaptic connections but also regulate the efficacy of synaptic transmission and plasticity (Bozdagi et al., 2004; Jungling et al., 2006; Okamura et al., 2004; Tanaka et al., 2000). Proteins assembled for the cadherin-mediated adherens junction have been extensively studied in various cell systems. However, different cadherins have been studied in distinct cell system models. Hence, it is unclear which proteins are genuinely assembled in synaptic junctions.

Cadherins are large superfamily of transmembrane cell adhesion proteins with characteristic extracellular repeats of about 110 amino acids. The cadherin superfamily comprises the classic cadherin and protocadherin subfamilies. Classic cadherins share conserved cytoplasmic domains that bind to β-catenin, whereas protocadherins have diversiform cytoplasmic domains connected to a wide variety of intracellular signaling molecules (Yagi and Takeichi, 2000). Classic cadherins are expressed in synaptic junctions (Benson and Tanaka, 1998; Fannon and Colman, 1996; Manabe et al., 2000; Uchida et al., 1996). Among them, N-cadherin

Abbreviations: AMPA, 2-amino-3-(5-methyl-3-oxo-1,2-oxazol-4-yl)propanoic acid; CNS, central nervous system; HBSS, Hanks' balanced salt solution; LC–MS/MS, liquid chromatography–tandem mass spectrometry; MAP kinase, mitogen-activated protein kinase; MT, microtubule; NMDA, *N*-methyl-D-aspartate; PAGE, polyacrylamide gel electrophoresis; PPW, presynaptic particle web; PSD, postsynaptic density; SDS, sodium dodecyl sulfate.

* Corresponding author. Address: Department of Pharmacology A6, Osaka University School of Medicine, 2-2 Yamadaoka, Suita, Osaka 565-0871, Japan. Tel.: +81 6 6879 3521; fax: +81 6 6879 3529.
E-mail address: htanaka@pharma1.med.osaka-u.ac.jp (H. Tanaka).

0197-0186/$ - see front matter © 2012 Elsevier Ltd. All rights reserved.
http://dx.doi.org/10.1016/j.neuint.2012.05.008

has been intensively investigated in hippocampal neurons and has been proven to play various roles in synaptic transmission and plasticity (Bozdagi et al., 2000; Jungling et al., 2006; Tang et al., 1998). The involvement of N-cadherin in synaptic activity is also supported by studies on cadherin-interacting proteins such as β-catenin (Okuda et al., 2007), δ-catenin (Israely et al., 2004), and IQ-GAP/ERK (Schrick et al., 2007).

Accumulating evidence indicates the involvement of N-cadherin as a dynamic feature of synaptic physiology. For example, N-cadherin mediates an activity-induced enlargement of the dendritic spine, which is dependent on rearrangement of the actin cytoskeleton (Okamura et al., 2004). Concomitantly, N-cadherin can undergo conformational change, e.g. dimerization, with acquired resistance to trypsin (Tanaka et al., 2000). At the same time, N-cadherin shows enhanced binding to β-catenin (Murase et al., 2002) and stabilization on the cell surface (Tai et al., 2007). The immobilization of N-cadherin/β-catenin parallels with the stabilization of actin filaments by synaptic stimulation (Fischer et al., 2000; Fukazawa et al., 2003; Lin et al., 2005; Okamoto et al., 2004; Star et al., 2002). There are also suggestions that the N-cadherin–catenin complex is more directly linked to presynaptic vesicular physiology (Bamji et al., 2003, 2006; Bozdagi et al., 2004; Jungling et al., 2006) as well as postsynaptic neurotransmitter receptors (Saglietti et al., 2007). Furthermore, there are pathways that force N-cadherin into intracellular compartments. One pathway involves steady-state endocytosis, which is inhibited by the activation of the NMDA receptor (Tai et al., 2007). Another is an activity-regulated endocytic pathway, in which arcadlin (protocadherin-8), induces endocytosis of N-cadherin as a downstream event of p38 MAP kinase activation (Yasuda et al., 2007).

Thus, N-cadherin plays multiple, dynamic roles in synaptic remodeling and plasticity. Synaptic N-cadherin should therefore be linked to distinct cellular mechanisms that are specialized for separate, specific tasks. Here, we focus on the rodent hippocampal synapse to directly depict the cadherin-mediated adhesion complex. We describe the proteomic assortment of the synaptic adhesion apparatus assisted by N-cadherin in cultured hippocampal neurons. The protein complexes assembled with N-cadherin were consistent with the N-cadherin linkages to F-actins, intermediate filaments, and microtubules. In addition, synaptic stimulation by membrane depolarization resulted in the increase of a 93-kDa band, which corresponded to proteolytically truncated β-catenin. The integration of three different cytoskeletal systems takes place in N-cadherin-mediated adhesive machinery, providing a dynamic scaffold underlying synaptic plasticity.

2. Materials and methods

2.1. Neuron culture

Hippocampal neurons were cultured from E18 rat embryos as previously described (Tanaka et al., 2000). Neurons were plated at a density of 1.4–2.1 × 10^4 cells/cm^2 onto poly-L-lysine-coated dishes (Φ = 35 mm). Neurons were maintained in Neurobasal medium supplemented with B27 (Life Technologies) and 5 μM cytosine arabinoside.

2.2. Protein extraction, immunoprecipitation, and immunoblotting

Hippocampi were dissected from adult C57BL/6 mice, homogenized in Ca-PI-lysis buffer (10 mM HEPES–NaOH (pH 7.4), 1% Triton X-100, 120 mM NaCl, 2 mM $CaCl_2$, 10 μg/ml leupeptin, 10 μg/ml pepstatin A, 1 μg/ml aprotinin, 0.2 mM phenylmethylsulfonyl fluoride, 20 mM NaF, 20 mM β-glycerophosphate, and 1 mM Na_3VO_4) with a Teflon-glass homogenizer, and centrifuged for 1 h to obtain clear protein extracts. Mature neurons cultured for 4–5 weeks were depolarized with 50 mM KCl for 15 min. Neurons were washed twice with chilled PBS, harvested with 80 μl (for a Φ = 35 mm dish) of Ca-PI-lysis buffer, sonicated, and centrifuged. N-cadherin-associated protein complex was immunoprecipitated from these samples with 0.5–2.5 μg of murine anti-N-cadherin (BD Transduction Laboratories). The precipitated protein complex was separated in 4–15% gradient SDS–PAGE followed by either silver staining, Sypro Ruby (Molecular Probes) staining, or immunoblotting. Immunoblots were probed with murine anti-α-catenin (BD Transduction Laboratories, 1:5000), murine anti-p120 (BD Transduction Laboratories, 1:2500), murine anti-plakoglobin (BD Transduction Laboratories, 1:2000), rabbit anti-syntaxin 1 (Sigma–Aldrich, 1:10000), rabbit anti-JLP (SPAG9) (Abcam, 1:10000), rabbit anti-pan-14-3-3 (Millipore, 1:5000), murine anti-TRAP1 (BD Transduction Laboratories 1:5000), rabbit anti-DDB1 (Abcam, 1:5000), and rabbit anti-TRIM33 (Bethyl Laboratories, 1:2000) antibodies.

2.3. Sequential extraction of synaptosome fractions

Hippocampi isolated from two mice were homogenized (Dounce homogenizer, 30 strokes) in buffered sucrose (0.32 M sucrose in hypotonic A buffer). Hypotonic A buffer contained 4 mM HEPES–NaOH (pH 7.4), 1 mM $MgCl_2$, 0.5 mM $CaCl_2$, and 0.0025% butylated hydroxy toluene. The homogenate was centrifuged (800g × 10 min) and the supernatant (S1) was centrifuged again (9200g × 15 min) to collect the precipitate (P2). The P2 pellet was resuspended in buffered sucrose and overlaid on stepwise sucrose gradients (0.85, 1.0, and 1.2 M) and ultracentrifuged at 82,500g for 120 min. The crude synaptosome fraction accumulated between 1.0 and 1.2 M cushions was collected, diluted with 3 × volume of hypotonic A buffer, and ultracentrifuged (32,800g × 20 min). The resultant synaptosome pellet was resuspended in 120 μl of isotonic buffer B (10 mM HEPES–NaOH (pH 7.4), 120 mM NaCl, 1 mM $MgCl_2$, 0.5 mM $CaCl_2$, 0.0025% butylated hydroxy toluene, 10 μg/ml leupeptin, 10 μg/ml pepstatin A, 1 μg/ml aprotinin, and 0.2 mM phenylmethylsulfonyl fluoride), mixed with 30 μl of 0.1 M methyl-β-cyclodextrin, and incubated at 37 °C for 15 min followed by centrifugation (15,000 rpm × 15 min at 23 °C). After removing the supernatant as a methyl-β-cyclodextrin extract, the pellet was resuspended in 150 μl of stripping buffer (5 M urea dissolved in isotonic buffer B) and centrifuged as previously to obtain a urea extract and stripped-membrane pellet. The urea-stripped membrane pellet was resuspended in 150 μl of solubilizing buffer (1% Triton X-100 dissolved in isotonic buffer B) and centrifuged to obtain a Triton extract and an insoluble pellet.

2.4. In-gel digestion

Gel pieces were excised from Sypro Ruby-stained gels and washed with 50% (v/v) acetonitrile and 50 mM NH_4HCO_3, pH 8.0, for 30 min to remove the fluorescence dye. Gel pieces were then soaked in acetonitrile for 5 min, acetonitrile was removed, and the gel pieces were dried for 20 min in a vacuum. Prior to enzymatic digestion, gel pieces were reduced with 10 mM dithiothreitol in 50 mM NH_4HCO_3 at 37 °C for 30 min, then alkylated with 55 mM iodoacetamide in 50 mM NH_4HCO_3 for 30 min, and dehydrated by addition of acetonitrile. The reduced and alkylated gel pieces were rehydrated in 50 mM Tris–HCl, pH 9.0, and 0.5 μg/ml sequencing grade modified trypsin (Roche Diagnostics). Once this solution was fully absorbed by the gel pieces, enzyme-free Tris–HCl buffer was added until the gel pieces were covered. The samples were digested for 16 h at 37 °C, extracted with acetonitrile and 5% formic acid for 20 min, and acetonitrile was evaporated using a Speed-Vac centrifuge. The tryptic digests were desalted

with C18-StageTips, concentrated using the Speed-Vac centrifuge, and reconstituted in 0.1% formic acid and 3% acetonitrile.

2.5. In-solution digestion for shotgun analyses

Immunoprecipitated samples were added to 50 mM Tris–HCl, pH 9.0, reduced with 10 mM dithiothreitol at 37 °C for 30 min, alkylated with 55 mM iodoacetamide in the dark at room temperature for 30 min, and digested with 0.5 μg/ml sequencing grade modified trypsin at 37 °C for 16 h. The digests were desalted and reconstituted as above.

2.6. LC–MS/MS and data analysis

LC–MS/MS analysis was performed by a Paradigm MS4 nano-HPLC system (Michrom BioResources, Inc., Auburn, CA) coupled to an LTQ linear ion trap mass spectrometer (Thermo Electron Corp., Waltham, MA) with a nanoelectrospray ionization source (AMR Inc., Tokyo, Japan). Tryptic peptides were injected by an HTC-PAL autosampler (CTC Analytics AG, Zwingen, Switzerland) and enriched on a C18 trap column (300 μm I.D. × 5 mm length, CERI, Tokyo, Japan) at a flow rate of 6 μl/min. The samples were subsequently separated by a C18 reverse phase column (100 μm I.D. × 150 mm length, Nikkyo Technos Co., Ltd., Tokyo, Japan) at a flow rate of 1 μl/min with a linear gradient from 2% to 65% mobile phase B, i.e. from 98% to 35% of mobile phase A. Mobile phase B consisted of 95% acetonitrile with 0.1% formic acid, whereas mobile phase A consisted of 2% acetonitrile with 0.1% formic acid. LC–MS/MS analysis was carried out using data-dependent triple-play mode. Automated gain control values were set at 1.5×10^4, 1.5×10^3, and 5.0×10^3 for Full-MS, Zoom-MS, and MS/MS, respectively. A spray voltage of 1.6 kV was applied. The MS scan range was *m/z* 300–2000. Peptides and proteins were identified by Mascot v2.2 (Matrix Science, London, UK) with a maximum tolerance of 1.2 Da for MS data, 0.5 Da for MS/MS data, and strict trypsin specificity allowing for up to one missed cleavage. Carbamidomethylation of cysteine and oxidation of methionine were allowed as a variable modification.

2.7. Trypsin treatment of living neurons

Modification of N-cadherin in response to synaptic stimulation was demonstrated by the acquired resistance to trypsin as reported (Tanaka et al., 2000). Stimulated and control neurons, maintained in 35 mm dishes (14,400 cells/cm^2), were washed briefly with prewarmed (37 °C) HEPES-buffered (10 mM, pH 7.4) HBSS and covered with 0.1% trypsin (Life Technologies) diluted with HBSS. The excess trypsin solution was removed immediately, followed by incubation for 10 min at 37 °C. The digested neurons were directly harvested in SDS–PAGE sample buffer (80 μl), or 40 μl of Ca-lysis buffer supplemented with soybean trypsin inhibitor (10 mM HEPES–NaOH (pH 7.4), 1% Triton X-100, 120 mM NaCl, 2 mM $CaCl_2$, 10 μg/ml leupeptin, 10 μg/ml pepstatin A, 1 μg/ml aprotinin, 0.2 mM phenylmethylsulfonyl fluoride, and 0.01% trypsin inhibitor) followed by centrifugation (15,000 rpm × 5 min at 4 °C) to obtain the Triton-soluble supernatant and the Triton-insoluble pellet. The supernatant was mixed with 5 × SDS–PAGE sample buffer (10 μl), and the pellet was resuspended in SDS–PAGE sample buffer containing 4 M urea (40 μl).

3. Results and discussion

3.1. Strategy

N-cadherin is expressed in synaptic membranes of hippocampal neurons (Benson and Tanaka, 1998; Tanaka et al., 2000). Synaptic N-cadherin appears to comprise: a surface pool in the endocytic zone located in the periphery of the synapse (Tanaka et al., 2000; Uchida et al., 1996), an intracellular pool such as endosomes (Tai et al., 2007; Yasuda et al., 2007), and an active zone pool associated with the presynaptic particle web (PPW) and postsynaptic density (PSD) (Fig. 1A) (Phillips et al., 2001).

The active zone-associated electron-dense structures (PPW + PSD), which correspond to so-called synaptic junctions, are biochemically characterized by the insolubility in 1% Triton X-100 (Phillips et al., 2001). Approximately 60% of N-cadherin was collected in the Triton-soluble fraction and 40% in the Triton-insoluble fraction (Fig. 1B,C). In the epithelial cells, the Triton-insoluble fraction is comprised of cytoskeleton-associated scaffolding protein complexes and cholesterol-rich lipid rafts (Brown and Rose, 1992). N-cadherin was not extracted from the crude synaptosome fraction with methyl-β-cyclodextrin, a cholesterol-extracting agent, suggesting that the Triton-insoluble N-cadherin is largely integrated into the synaptic junctional complex (Fig. 1B,C). Usually, biochemical analyses of the synaptic junctions utilize these Triton-insoluble PSD fractions (Cotman et al., 1974). For example, in immunoprecipitation experiments, the PSD is solubilized with high concentration of ionic detergent (e.g., 10% sodium deoxycholate), and then the detergent is diluted, so that the disrupted proteins may reassemble, allowing the reassembled protein complexes to be co-immunoprecipitated (Luo et al., 1997).

The surface endocytic zone and endosome pools of N-cadherin (Fig. 1A (1) and (2)) are also supposed to be involved in the plasticity of synaptic structures, and are largely soluble in 1% Triton X-100 by several reasons. First, the surface pools undergo vigorous redistributions by synaptic acitivity (Okamura et al., 2004; Tanaka et al., 2000). These mobile pools were extractable with 1% Triton X-100 in our unpublished observations. Second, the endocytosed N-cadherin is shown to be extracted with 1% Triton X-100/0.1% SDS as detected in western blotting (Tai et al., 2007). Third, the synaptic stimulation-induced trypsin-resistance of N-cadherin was readily detectable in the Triton-soluble fraction as well as in the Triton-insoluble fraction (Fig. 1D). The acquired trypsin-resistance of N-cadherin is a sign of conformational change in response to synaptic activity, and this implies rearrangements of protein–protein interactions (Tanaka et al., 2000).

Thus we reasoned that the determination of protein–protein interactions within the Triton-soluble fraction from synapse-enriched neuronal lysate provides insight into the mechanisms involved in the dynamism of the synaptic structure. There are several advantages by focusing on the Triton-soluble fraction. First, we are able to avoid artificial disruption/reassembly of protein complexes with ionic detergent and its dilution. The intrinsic interactions are directly captured by one-step lysis with Triton X-100. Second, Triton X-100 is a non-ionic detergent and expected to maintain relatively weak protein–protein interactions. The expected disadvantage is that this approach fails to detect the strong protein–protein interactions that involve scaffolding proteins within the PSD.

We used rat hippocampal neurons cultured for 5–6 weeks. Neurons at this stage develop enormous numbers of mature synaptic junctions that are positive for N-cadherin with little contamination by glial cells (Tanaka et al., 2000). Most N-cadherin-positive synaptic puncta cluster at PSD-95-containing postsynaptic densities, a marker of excitatory synapses, but not at GABAergic termini (Benson and Tanaka, 1998). After solubilizing the neurons with 1% Triton X-100, N-cadherin was immunoprecipitated and subjected to SDS–PAGE (Fig. 2A). The bands in the gel specific for anti-N-cadherin antibody but not for control IgG were excised and subjected to in-gel digestion followed by LC–MS/MS analysis (Fig. 2B, Table 1).

We also performed shotgun LC–MS/MS analysis of murine hippocampal extracts in the same buffer conditions. In these